Journal of Computational Physics 325 (2016) 74–97

Contents lists available at ScienceDirect

Journal of Computational Physics

www.elsevier.com/locate/jcp

On the ground states and dynamics of space fractional nonlinear Schrödinger/Gross–Pitaevskii equations with rotation term and nonlocal nonlinear interactions

Xavier Antoine [a], Qinglin Tang [a,b,*], Yong Zhang [c,d]

[a] Institut Elie Cartan de Lorraine, Université de Lorraine, Inria Nancy-Grand Est, F-54506 Vandoeuvre-lès-Nancy Cedex, France
[b] Laboratoire de Mathématiques Raphaël Salem, Université de Rouen, Technopôle du Madrillet, 76801 Saint-Etienne-du-Rouvray, France
[c] Université de Rennes 1, IRMAR, Campus de Beaulieu, 35042 Rennes Cedex, France
[d] Wolfgang Pauli Institute c/o Fak. Mathematik, University Wien, Oskar-Morgenstern-Platz 1, 1090 Vienna, Austria

ARTICLE INFO

Article history:
Received 8 December 2015
Received in revised form 18 April 2016
Accepted 9 August 2016
Available online 24 August 2016

Keywords:
Fractional Schrödinger equation
Rotation
Nonlocal nonlinear interaction
Rotating Lagrangian coordinates
Gaussian-sum solver
Ground state
Dynamics

ABSTRACT

In this paper, we propose some efficient and robust numerical methods to compute the ground states and dynamics of Fractional Schrödinger Equation (FSE) with a rotation term and nonlocal nonlinear interactions. In particular, a newly developed Gaussian-sum (GauSum) solver is used for the nonlocal interaction evaluation [31]. To compute the ground states, we integrate the preconditioned Krylov subspace pseudo-spectral method [4] and the GauSum solver. For the dynamics simulation, using the rotating Lagrangian coordinates transform [14], we first reformulate the FSE into a new equation without rotation. Then, a time-splitting pseudo-spectral scheme incorporated with the GauSum solver is proposed to simulate the new FSE. In parallel to the numerical schemes, we also prove some existence and nonexistence results for the ground states. Dynamical laws of some standard quantities, including the mass, energy, angular momentum and the center of mass, are stated. The ground states properties with respect to the fractional order and/or rotating frequencies, dynamics involving decoherence and turbulence together with some interesting phenomena are reported.

1. Introduction

Recently, a great deal of attention has been directed towards the derivation of a powerful generalization of PDEs through the inclusion of fractional order operators [26,35,42,51]. The aim of this paper is to contribute to this new hot area for fractional quantum physics, with possible applications, e.g. in Bose–Einstein condensation (BEC). During the last decades, the classical Schrödinger Equation (SE) has been widely investigated and applied to many areas in physics (optics, electromagnetic, superfluidity, etc.). It is known as the fundamental equation of classical quantum mechanics which can be interpreted by the Feynman path integral approach over Brownian-like quantum paths [32]. Lately, Laskin extended the Feynman path integral approach over the more general Lévy-like quantum paths and derived a Fractional Schrödinger Equation (FSE), which modifies the SE by involving the fractional Laplacian $(-\Delta)^s$ [46–48]. The FSE was then applied to represent the Bohr

* Corresponding author at: Institut Elie Cartan de Lorraine, Université de Lorraine, Inria Nancy-Grand Est, F-54506 Vandoeuvre-lès-Nancy Cedex, France.
E-mail addresses: xavier.antoine@univ-lorraine.fr (X. Antoine), qinglin.tang@inria.fr (Q. Tang), yong.zhang@univ-rennes1.fr (Y. Zhang).
URL: http://iecl.univ-lorraine.fr/~xantoine/ (X. Antoine).

http://dx.doi.org/10.1016/j.jcp.2016.08.009
0021-9991/

atom, fractional oscillator [48], and it is a new fractional approach to study the quantum chromodynamics (QCD) problem of quarkonium [46]. The FSE also arises in the continuum limit of the discrete SE with long-range dispersive interaction [43], in the mathematical description of boson stars [28] and in some models of water wave dynamics [39]. It has also been proposed to study BEC of which the particles obey a non-Gaussian distribution law [30,56,57], where FSE was named as Fractional Gross–Pitaevskii Equation (FGPE) and BEC as Fractional BEC (FBEC). Compared with the SE, the literature on FSE is quite limited but growing quickly to understand its mathematical and physical properties.

More precisely, we consider here the following generalized dimensionless (space-) Fractional NonLinear Schrödinger equation (FNLSE) with a rotation term and a nonlocal nonlinear interaction

$$i\partial_t \psi(\mathbf{x},t) = \left[\frac{1}{2}\left(-\nabla^2+m^2\right)^s + V(\mathbf{x}) + \beta|\psi(\mathbf{x},t)|^2 + \lambda\Phi(\mathbf{x},t) - \Omega L_z\right]\psi(\mathbf{x},t), \tag{1.1}$$

$$\Phi(\mathbf{x},t) = \mathcal{U} * |\psi(\mathbf{x},t)|^2, \qquad \mathbf{x}\in\mathbb{R}^d,\ t>0,\ d\geq 2. \tag{1.2}$$

In the context of BEC, this equation is also called as FGPE. Here, $\psi(\mathbf{x},t)$ is the complex-valued wave-function, $t>0$ is the time variable and $\mathbf{x}\in\mathbb{R}^d$ is the spatial coordinate. The constant $m\geq 0$ denotes the scaled particle mass, with $m=0$ representing the massless particle. The parameter $s>0$ is the space fractional order characterizing the nonlocal dispersive interaction. Hereafter, we call the fractional dispersion as *superdispersion* (*subdispersion*) for $s>1$ ($s<1$). In addition, the fractional kinetic operator is defined *via* a Fourier integral operator

$$\left(-\nabla^2+m^2\right)^s \psi = \frac{1}{(2\pi)^d}\int_{\mathbb{R}^d} \widehat{\psi}(\mathbf{k})\,(|\mathbf{k}|^2+m^2)^s e^{i\mathbf{k}\cdot\mathbf{x}} d\mathbf{k}, \tag{1.3}$$

where the Fourier transform is given by $\widehat{\psi}(\mathbf{k}) = \int_{\mathbb{R}^d}\psi(\mathbf{x})e^{-i\mathbf{k}\cdot\mathbf{x}}d\mathbf{x}$. The potential $V(\mathbf{x})$ is supposed to be trapping, a standard example being the harmonic potential given by

$$V(\mathbf{x}) = \begin{cases} \frac{\gamma_x^2x^2+\gamma_y^2y^2}{2}, & d=2,\\ \frac{\gamma_x^2x^2+\gamma_y^2y^2+\gamma_z^2z^2}{2}, & d=3, \end{cases} \tag{1.4}$$

where γ_v ($v=x,y,z$) is the trapping frequency in the v-direction. The real-valued constants β and λ characterize the local and nonlocal interaction strengths (positive/negative for repulsive/attractive interaction), respectively. The local interaction is supposed to be cubic, but other choices may also be considered. Concerning the nonlocal interaction (1.2), the convolution kernel $\mathcal{U}(\mathbf{x})$ can be chosen as either the kernel of a Coulomb-type interaction or a Dipole–Dipole Interaction (DDI) [13,16,21]

$$\mathcal{U}(\mathbf{x}) = \begin{cases} \frac{1}{2^{d-1}\pi|\mathbf{x}|^\mu}, & 0<\mu\leq d-1,\\ -\delta(\mathbf{x}) - 3\,\partial_{\mathbf{nn}}\left(\frac{1}{4\pi|\mathbf{x}|}\right), & \\ -\frac{3}{2}\left(\partial_{\mathbf{n}_\perp\mathbf{n}_\perp} - n_3^2\nabla_\perp^2\right)\left(\frac{1}{2\pi|\mathbf{x}|}\right), & \end{cases} \iff \widehat{\mathcal{U}}(\mathbf{k}) = \begin{cases} \frac{C}{|\mathbf{k}|^{d-\mu}}, & 0<\mu\leq d-1,\ \text{Coulomb},\\ -1+\frac{3(\mathbf{n}\cdot\mathbf{k})^2}{|\mathbf{k}|^2}, & \text{3D DDI},\\ \frac{3[(\mathbf{n}_\perp\cdot\mathbf{k})^2-n_3^2|\mathbf{k}|^2]}{2|\mathbf{k}|}, & \text{2D DDI}, \end{cases} \tag{1.5}$$

where $C=\pi^{d/2-1}2^{1-\mu}\Gamma(\frac{d-\mu}{2})/\Gamma(\frac{\mu}{2})$ ($\Gamma(t):=\int_0^\infty x^{t-1}e^{-x}dx$ is the Gamma function), $\mathbf{n}=(n_1,n_2,n_3)^T\in\mathbb{R}^3$ is a unit vector representing the dipole orientation and $\mathbf{n}_\perp=(n_1,n_2)^T$. In addition, $L_z=-i(x\partial_y-y\partial_x)=-i\partial_\theta$ is the z-component of the angular momentum, Ω represents the rotating frequency.

The FNLSE conserves two important physical quantities (see Section 4.1): the *mass*

$$\mathcal{N}(\psi(\cdot,t)) := \mathcal{N}(t) := \int_{\mathbb{R}^d}|\psi(\mathbf{x},t)|^2 d\mathbf{x} \equiv \mathcal{N}(0), \tag{1.6}$$

and the *energy*

$$\mathcal{E}(\psi(\cdot,t)) =: \mathcal{E}(t) = \int_{\mathbb{R}^d}\left[\frac{1}{2}\bar{\psi}\left(-\nabla^2+m^2\right)^s\psi + V(\mathbf{x})|\psi|^2 + \frac{\beta}{2}|\psi|^4 + \frac{\lambda}{2}\Phi|\psi|^2 - \Omega\bar{\psi}L_z\psi\right] \equiv \mathcal{E}(0). \tag{1.7}$$

Here, $\bar{\psi}$ is the complex conjugate of ψ. The ground states $\phi_g(\mathbf{x})$ of the FNLSE (1.1) are defined by

$$\phi_g(\mathbf{x}) = \arg\min_{\phi\in S}\mathcal{E}(\phi), \qquad S=\{\phi\in\mathbb{C}|\ \|\phi\|_2=1, \mathcal{E}(\phi)<\infty\}, \tag{1.8}$$

where $\|\phi\|_2$ is the $L^2(\mathbb{R}^d)$-norm of ϕ.

The FNLSE (1.1) brings together a wide range of Schrödinger-type PDEs. When $s=1$ and $m=0$, FNLSE reduces to the standard nonlinear Schrödinger equation (NLSE), which has been extensively studied both theoretically and numerically [2,3,5–7,9,12–16,20,25]. For $s\in(0,1)$ and Φ taken as the Coulomb potential, (1.1) reduces to the generalized semi-relativistic Hartree equation. The corresponding Cauchy problem (for $s\in[\frac{1}{2},1]$) as well as its ground state properties (for $s=\frac{1}{2}$)

have been partially investigated [1,21,23,24,28,34]. Nevertheless, to the best of our knowledge, there are neither theoretical nor numerical studies on the ground state properties for $s > 0$ other than the cases $s = 1/2$ and 1. When $s \in (0, 1)$ and $m = \lambda = \Omega = 0$, it reduces to the FNLSE that is originally derived by Laskin [46]. Since then, the FNLSE has attracted an increasing attention. Stationary states and dynamics properties have been partially considered in some special cases. We refer to [22,38,52–54] and references therein for more details. For the *superdispersion* case, i.e. $s > 1$, there are few Schrödinger-type equations, while it is quite common for the superdiffusion equations [37]. We consider here this case for some possible eventual physical applications.

In general, it is difficult to obtain analytical solutions for the FNLSE. Even for the simplest case with a box potential, there is still a controversy over the eigenpair solutions [17,18,36,40]. Therefore, to develop accurate numerical methods is quite crucial. So far there are very limited numerical studies. When $\Omega = \lambda = 0$, finite difference (FD) scheme [58] and Fourier pseudo-spectral method [27,44,45] were proposed to study the dynamics. When the nonlocal interaction is present (i.e. $\lambda \neq 0$), for the 3D semi-relativistic Hartree equation, Bao and Dong [11] proposed a sine pseudo-spectral method to compute its ground states and dynamics, where the nonlocal Coulomb potential Φ (1.2) satisfies the following Poisson equation

$$-\Delta\Phi = |\psi|^2, \ \mathbf{x} \in \mathbb{R}^3, \quad \text{with} \quad \lim_{|\mathbf{x}|\to\infty} \Phi(\mathbf{x}) = 0. \tag{1.9}$$

Similar ideas were applied to nonlocal DDI in NLSE [9,10]. However, due to the slow polynomial decay of Φ at the far-field, a quite large computational domain is necessary to guarantee a satisfactory accuracy. Up to now, most existing numerical methods are proposed for non-rotating FNLSE with $s \leq 1$. As far as we know, there were neither theoretical nor numerical methods for the generalized FNLSE (1.1) for $s \neq 1$ and $\lambda\Omega \neq 0$. The difficulties to develop an accurate and efficient scheme lie in the evaluation of the nonlocal interaction Φ (1.2) and proper treatment of the rotation term $L_z\psi$.

To compute the nonlocal interaction, Jiang et al. [41] proposed an accurate NonUniform Fast Fourier Transform (NUFFT)-based algorithm which is within $O(N \log N)$ arithmetic operations (N is the total number of grid points). This solver is more accurate than the PDE approach (1.9) and has been recently applied in the study of the ground state and dynamics of NLSE [13,16]. Recently, by approximating the kernel $\mathcal{U}(\mathbf{x})$ with the summation of a finite number of Gaussians, Zhang et al. [31] proposed a Gaussian-sum (GauSum)-based method, which improves the efficiency compared with NUFFT-based algorithm meanwhile maintains the spectral accuracy. Concerning the rotation term, Antoine and Duboscq [4,7] proposed a robust preconditioned Krylov subspace spectral solver for ground states computation of the NLSE with large Ω and β. For the dynamics, Bao et al. [14] developed a rotating Lagrangian coordinates transformation method to reformulate the rotating term into a time-dependent trapping potential, which allows for the implementation of high-order time-splitting schemes [19].

The main objectives of this paper are threefold.

1. Investigate theoretically the existence of the ground states of the general FNLSE (1.1) with respect to the fractional order s and the rotation speed Ω. Develop the dynamical laws for the center of mass as well as other standard dynamical quantities for general s and Ω, and compare them with those derived in [44].
2. Develop some efficient and accurate numerical methods for computing the ground states and dynamics of the general FNLSE (1.1) by incorporating the GauSum solver into the adapted version of the gradient flow and time-splitting Fourier pseudo-spectral method. The preconditioned Krylov subspace iteration [4] and the rotating Lagrangian transformation technique [14] will be also integrated into the numerical methods for the ground state computation and dynamics simulation, respectively.
3. Apply our numerical methods to study some interesting problems, e.g., the influence of the nonlocal dispersion on the ground states and on the dynamics such as chaos and decoherence.

The rest of the paper is organized as follows. In Section 2, we briefly review the Gaussian Sum method. The ground state computation, including the ground states properties and numerical methods as well as numerical results, are presented in Section 3. In Section 4, we derive some dynamical laws for some global physical quantities that are usually considered for the standard NLSE. We then propose an efficient and robust numerical method for the dynamics simulation. Some numerical results are also reported. Finally, a conclusion and some discussions are developed in Section 5.

2. Brief review of the Gaussian-Sum (GauSum) method

With the strong confining potential, the density $\rho := |\psi|^2$ is smooth and decays exponentially fast. Therefore, we can reasonably truncate the whole space to a bounded domain, e.g., a square box $\mathbf{B}_L := [-L, L]^d$. The density is then rescaled to be compactly supported in a unit box $\mathbf{B}_1$, which is now the computational domain. One of the key ideas is to use a GauSum approximation of the kernel $\mathcal{U}$ (see U_{GS} in (2.5)) to reformulate the potential into two integrals, namely, the *long-range regular integral* and the *short-range singular integral*. To be precise, we can reformulate the potential (1.2) as follows

$$\Phi(\mathbf{x}) \approx \int_{\mathbf{B}_1} \mathcal{U}(\mathbf{x}-\mathbf{y})\, \rho(\mathbf{y}) d\mathbf{y} = \int_{\mathbf{B}_2} \mathcal{U}(\mathbf{y})\, \rho(\mathbf{x}-\mathbf{y}) d\mathbf{y} \tag{2.1}$$

$$= \int_{\mathbf{B}_2} U_{\mathrm{GS}}(\mathbf{y})\, \rho(\mathbf{x}-\mathbf{y})d\mathbf{y} + \int_{\mathcal{B}_\delta} \big(\mathcal{U}(\mathbf{y}) - U_{\mathrm{GS}}(\mathbf{y})\big)\, \rho(\mathbf{x}-\mathbf{y})d\mathbf{y} + I_\delta \tag{2.2}$$

$$:= I_1(\mathbf{x}) + I_2(\mathbf{x}) + I_\delta, \qquad \mathbf{x} \in \mathbf{B}_1, \tag{2.3}$$

where

$$I_\delta = \int_{\mathbf{B}_2 \setminus \mathcal{B}_\delta} \big(\mathcal{U}(\mathbf{y}) - U_{\mathrm{GS}}(\mathbf{y})\big)\, \rho(\mathbf{x}-\mathbf{y})d\mathbf{y}, \tag{2.4}$$

with $\mathcal{B}_\delta := \{\mathbf{x} \big| |\mathbf{x}| \le \delta\}$ being a small neighborhood of the origin with radius $\delta \sim 10^{-4} - 10^{-3}$ and U_{GS} is given explicitly as follows

$$U_{\mathrm{GS}}(\mathbf{y}) = U_{\mathrm{GS}}(|\mathbf{y}|) := \sum_{q=0}^{Q} w_q\, e^{-\tau_q^2 |\mathbf{y}|^2}, \quad Q \in \mathbb{N}^+, \tag{2.5}$$

with weights and nodes $\{(w_q, \tau_q)\}_{q=0}^{Q}$. Here, U_{GS} designates an accurate approximation of $\mathcal{U}$, up to $\varepsilon_0 \sim 10^{-14} - 10^{-16}$, within the interval $[\delta, 2]$, i.e.

$$\|\mathcal{U}(r) - U_{\mathrm{GS}}(r)\|_{L^\infty([\delta,2])} \le \varepsilon_0. \tag{2.6}$$

For (2.4), we have $|I_\delta| \le C\varepsilon_0\, \delta^d\, \|\rho\|_{L^\infty}$. Thus the remainder integral I_δ is negligible and is omitted here. Note that the GauSum approximation can be numerically computed with *sinc quadrature* and we refer to [31] for more details.

To compute the *regular integral* I_1, plugging the explicit GauSum approximation (2.5) into $I_1(\mathbf{x})$ yields

$$I_1(\mathbf{x}) = \sum_{q=0}^{Q} w_q \int_{\mathbf{B}_2} e^{-\tau_q^2 |\mathbf{y}|^2} \rho(\mathbf{x}-\mathbf{y})d\mathbf{y}, \qquad \mathbf{x} \in \mathbf{B}_1. \tag{2.7}$$

For $\mathbf{x} \in \mathbf{B}_1$ and $\mathbf{y} \in \mathbf{B}_2$, we have $\mathbf{x} - \mathbf{y} \in \mathbf{B}_3$. We then can approximate $\rho(\mathbf{x}-\mathbf{y})$ on $\mathbf{B}_3$ by finite Fourier series. More precisely, ρ can be well approximated by Fourier series after zero-padding to $\mathbf{B}_3$ as follows

$$\rho(\mathbf{z}) \approx \sum_{\mathbf{k}} \widehat{\rho}_{\mathbf{k}} \prod_{j=1}^{d} e^{\frac{2\pi i k_j}{b_j - a_j}(z_j - a_j)}, \qquad \mathbf{z} = (z_1, \ldots, z_d) \in \mathbf{B}_3, \tag{2.8}$$

where $a_j = -3, b_j = 3$, $j = 1, \ldots, d$ and $\mathbf{k} \in \mathbb{Z}^d$. After some careful calculations, we have

$$I_1(\mathbf{x}) = \sum_{\mathbf{k}} \widehat{\rho}_{\mathbf{k}} \left(\sum_{q=0}^{Q} w_q G_{\mathbf{k}}^q \right) \prod_{j=1}^{d} e^{\frac{2\pi i k_j}{b_j - a_j}(x_j - a_j)}, \tag{2.9}$$

where

$$G_{\mathbf{k}}^q = \prod_{j=1}^{d} \int_{-2}^{2} e^{-\tau_q^2 |y_j|^2} e^{\frac{-2\pi i k_j y_j}{b_j - a_j}} dy_j = \prod_{j=1}^{d} \int_{0}^{2} 2\, e^{-\tau_q^2 |y_j|^2} \cos(\tfrac{2\pi k_j y_j}{b_j - a_j}) dy_j, \tag{2.10}$$

can be pre-computed once for all if the potential is computed on the same grid.

For the *near-field correction integral* I_2, within the small ball $\mathcal{B}_\delta$, the density function $\rho_{\mathbf{x}}(\mathbf{y}) := \rho(\mathbf{x}-\mathbf{y})$ is approximated by a low-order Taylor expansion as follows

$$\begin{aligned} \rho_{\mathbf{x}}(\mathbf{y}) \approx \mathrm{P}_{\mathbf{x}}(\mathbf{y}) &= \rho_{\mathbf{x}}(\mathbf{0}) + \sum_{j=1}^{d} \frac{\partial \rho_{\mathbf{x}}(\mathbf{0})}{\partial y_j} y_j + \frac{1}{2} \sum_{j,k=1}^{d} \frac{\partial^2 \rho_{\mathbf{x}}(\mathbf{0})}{\partial y_j \partial y_k} y_j\, y_k + \frac{1}{6} \sum_{j,k,\ell=1}^{d} \frac{\partial^3 \rho_{\mathbf{x}}(\mathbf{0})}{\partial y_j \partial y_k \partial y_\ell} y_j\, y_k\, y_\ell \\ &= \rho(\mathbf{x}) + \sum_{j=1}^{d} (\partial_{y_j} \rho)(\mathbf{x}) y_j + \frac{1}{2} \sum_{j,k=1}^{d} (\partial_{y_j y_k} \rho)(\mathbf{x}) y_j\, y_k + \frac{1}{6} \sum_{j,k,\ell=1}^{d} (\partial_{y_j y_k y_\ell} \rho)(\mathbf{x}) y_j\, y_k\, y_\ell. \end{aligned} \tag{2.11}$$

The derivatives involved are computed by differentiating the density's Fourier series approximation. Next, we replace $\rho_{\mathbf{x}}(\mathbf{y})$ by its Taylor approximation $\mathrm{P}_{\mathbf{x}}(\mathbf{y})$ and integrate in spherical/polar coordinates. The computation boils down to a multiplication of the Laplacian $\Delta\rho$ since the contributions of the odd-order derivatives in (2.11) and off-diagonal components of the Hessian vanish. To be precise, we first present for the 2D Coulomb potential case. Starting from the density's Fourier series approximation

$$\rho(\mathbf{x}) = \sum_{\mathbf{k}} \widehat{\rho}_{\mathbf{k}}\, e^{\frac{i\,2\pi k_1 (x+3)}{6}} e^{\frac{i\,2\pi k_2 (y+3)}{6}} =: \sum_{\mathbf{k}} \widehat{\rho}_{\mathbf{k}}\, \omega_{k_1}(x)\, \omega_{k_2}(y), \quad \mathbf{x} \in \mathbf{B}_3, \tag{2.12}$$

by differentiating (2.12), we obtain the derivatives in (2.11). For example, we get $\partial_{xy}\rho$ as follows

$$\partial_{xy}\rho(\mathbf{x}) = \sum_{\mathbf{k}} \widehat{\rho}_{\mathbf{k}}\, \mu_{k_1}\mu_{k_2}\, \omega_{k_1}(x)\, \omega_{k_2}(y), \quad \text{with} \quad \mu_{k_j} = i\,2\pi k_j/6,\ j = 1, 2. \tag{2.13}$$

All the other coefficients are computed likewise. Replace $\rho_{\mathbf{x}}$ in (2.3) by its Taylor approximation $\mathrm{P}_{\mathbf{x}}(\mathbf{y})$ and integrate with respect to $\mathbf{y}$, we have

$$\begin{aligned} I_2(\mathbf{x}) &\approx \int_{\mathcal{B}_\delta} \big(\mathcal{U}(\mathbf{y}) - U_{\mathrm{GS}}(\mathbf{y})\big)\, \mathrm{P}_{\mathbf{x}}(\mathbf{y}) d\mathbf{y} := \int_{\mathcal{B}_\delta} D_{\mathrm{GS}}(\mathbf{y})\, \mathrm{P}_{\mathbf{x}}(\mathbf{y}) d\mathbf{y} \\ &= \rho(\mathbf{x}) \int_{\mathcal{B}_\delta} D_{\mathrm{GS}}(\mathbf{y}) d\mathbf{y} + \sum_{j=1}^{2} (\partial_{y_j}\rho)(\mathbf{x}) \int_{\mathcal{B}_\delta} D_{\mathrm{GS}}(\mathbf{y})\, y_j d\mathbf{y} \\ &\quad + \frac{1}{2} \sum_{j,k=1}^{2} (\partial_{y_j y_k}\rho)(\mathbf{x}) \int_{\mathcal{B}_\delta} D_{\mathrm{GS}}(\mathbf{y})\, y_j y_k d\mathbf{y} + \frac{1}{6} \sum_{j,k,\ell=1}^{d} (\partial_{y_j y_k y_\ell}\rho)(\mathbf{x}) \int_{\mathcal{B}_\delta} D_{\mathrm{GS}}(\mathbf{y})\, y_j\, y_k\, y_\ell d\mathbf{y}, \end{aligned}$$

where $D_{\mathrm{GS}}(\mathbf{y}) := \mathcal{U}(\mathbf{y}) - U_{\mathrm{GS}}(\mathbf{y})$ is radial symmetric. All the odd-order derivative terms vanish because the corresponding integrands are all anti-symmetric, and I_2 evaluation comes down to a summation of the even-order derivative terms. For the second-order derivatives, the integral corresponding to $\partial_{xy}\rho$ vanishes for the same reason. Finally, we have

$$I_2(\mathbf{x}) \approx \rho(\mathbf{x}) \int_{\mathcal{B}_\delta} D_{\mathrm{GS}}(\mathbf{y}) d\mathbf{y} + \frac{1}{2}\Big(\partial_{xx}\rho(\mathbf{x}) \int_{\mathcal{B}_\delta} D_{\mathrm{GS}}(\mathbf{y})\, x^2 d\mathbf{y} + \partial_{yy}\rho(\mathbf{x}) \int_{\mathcal{B}_\delta} D_{\mathrm{GS}}(\mathbf{y})\, y^2 d\mathbf{y}\Big) \tag{2.14}$$

$$= \rho(\mathbf{x}) \int_{\mathcal{B}_\delta} D_{\mathrm{GS}}(\mathbf{y}) d\mathbf{y} + \frac{1}{2}(\Delta\rho)(\mathbf{x}) \int_{\mathcal{B}_\delta} D_{\mathrm{GS}}(\mathbf{y})\, x^2 d\mathbf{y}, \qquad \mathbf{x} \in \mathbb{R}^2. \tag{2.15}$$

The last identity holds because $\int_{\mathcal{B}_\delta} D_{\mathrm{GS}}(\mathbf{y}) x^2 d\mathbf{y} = \int_{\mathcal{B}_\delta} D_{\mathrm{GS}}(\mathbf{y}) y^2 d\mathbf{y}$. The two integrals in (2.15) are precomputed analytically once for all in polar coordinates. The I_2 evaluation comes down to a summation of the density and its Laplacian. As for the 3D Coulomb potential case, I_2 can be computed in a similar way as the 2D case. After plugging Taylor expansion approximation $P_{\mathbf{x}}(\mathbf{y})$ and integrating over $\mathcal{B}_\delta \subset \mathbb{R}^3$, we have

$$I_2(\mathbf{x}) \approx \rho(\mathbf{x}) \int_{\mathcal{B}_\delta} D_{\mathrm{GS}}(\mathbf{y}) d\mathbf{y} + \frac{1}{2}(\Delta\rho)(\mathbf{x}) \int_{\mathcal{B}_\delta} D_{\mathrm{GS}}(\mathbf{y})\, x^2 d\mathbf{y}, \qquad \mathbf{x} \in \mathbb{R}^3. \tag{2.16}$$

The GauSum method achieves a spectral accuracy and is essentially as efficient as FFT algorithms within $O(N \log N)$ arithmetic operations. The algorithm was implemented for the Coulomb-type kernels in [31]. The evaluations of 2D and 3D DDIs boil down to the Coulomb potential evaluation with modified densities. More explicitly, the DDIs can be reformulated as follows

$$\Phi(\mathbf{x}) = -\frac{3}{2}\left(\partial_{\mathbf{n}_\perp\mathbf{n}_\perp} - n_3^2\nabla_\perp^2\right)\left(\frac{1}{2\pi|\mathbf{x}|}\right) * \rho = \left(\frac{1}{2\pi|\mathbf{x}|}\right) * \left(-\frac{3}{2}(\partial_{\mathbf{n}_\perp\mathbf{n}_\perp}\rho - n_3^2\nabla_\perp^2\rho)\right), \ \mathbf{x} \in \mathbb{R}^2, \tag{2.17}$$

$$\Phi(\mathbf{x}) = -(\mathbf{n}\cdot\mathbf{n})\rho(\mathbf{x}) + \partial_{\mathbf{nn}}\left(\frac{1}{4\pi|\mathbf{x}|}\right) * \rho = -(\mathbf{n}\cdot\mathbf{n})\rho(\mathbf{x}) + \frac{1}{4\pi|\mathbf{x}|} * (\partial_{\mathbf{nn}}\rho), \quad \mathbf{x} \in \mathbb{R}^3. \tag{2.18}$$

To compute the DDIs, we just need to substitute the modified densities, i.e. $-\frac{3}{2}(\partial_{\mathbf{n}_\perp\mathbf{n}_\perp}\rho - n_3^2\nabla_\perp^2\rho)$ and $(\partial_{\mathbf{nn}}\rho)$ for ρ in (2.1) for the 2D and 3D cases, respectively. The modified densities are also computed via a similar Fourier series approximation procedure as shown in (2.13).

3. Ground state computation: properties, numerical scheme and simulations

In this section, we first prove some results related to the existence/non-existence of the ground states (subsection 3.1). We next propose in subsection 3.2 an efficient and accurate numerical method for computing the ground states by combining the normalized gradient flow which is discretized by the semi-implicit backward Euler Fourier pseudo-spectral method and the Gaussian-Sum nonlocal interaction solver. We shall refer to this new method as *GF-GauSum* hereafter. Finally, subsection 3.3 reports some results on the ground states to show some special features related to FNLSEs.

3.1. Existence and nonexistence of the ground states

To simplify the presentation, we divide the energy functional $\mathcal{E}(\phi)$ (1.7) into five parts, i.e. the kinetic, potential, rotating, local and nonlocal interactions energy parts

$$\mathcal{E}(\phi(\mathbf{x})) = \mathcal{E}_{\rm kin}(\phi) + \mathcal{E}_{\rm pot}(\phi) + \mathcal{E}_{\rm rot}(\phi) + \mathcal{E}_{\rm int}(\phi) + \mathcal{E}_{\rm non}(\phi), \tag{3.1}$$

where

$$\mathcal{E}_{\rm kin}(\phi) := \frac{1}{2}\Big\langle \big(-\nabla^2 + m^2\big)^s \phi, \phi \Big\rangle, \qquad \mathcal{E}_{\rm pot}(\phi) := \langle V(\mathbf{x})\phi, \phi\rangle,$$
$$\mathcal{E}_{\rm rot}(\phi) = -\Omega\langle L_z\phi, \phi\rangle, \quad \mathcal{E}_{\rm int}(\phi) := \frac{\beta}{2}\langle |\phi|^2, |\phi|^2\rangle, \quad \mathcal{E}_{\rm non}(\phi) := \frac{\lambda}{2}\langle \Phi, |\phi|^2\rangle,$$

with $\langle f, g\rangle = \int_{\mathbb{R}^d} f\,\bar{g}\,d\mathbf{x}$. We first prove some properties of the energy functional $\mathcal{E}(\phi(\mathbf{x}))$ for any $\phi \in S$.

Lemma 3.1. *If the convolution kernel $\mathcal{U}(\mathbf{x})$ in (1.5) is chosen as the Coulomb-type interaction and V is the harmonic potential defined by (1.4), we have the following properties*

(i) *For any positive $\varepsilon > 0$, we have for $\phi \in S$*

$$\Big|\big\langle \Phi, \rho\big\rangle\Big| = \Big|\big\langle \mathcal{U}(\mathbf{x}) * \rho, \rho\big\rangle\Big| \le \varepsilon \|\nabla\phi\|_2^2 + C_\varepsilon, \tag{3.2}$$

where C_ε is a real-valued constant that depends only on d, μ and ε.

(ii) *When $s > 1$, for any $m \ge 0$ and $\phi \in S$, we have*

$$\int_{\mathbb{R}^d} \Big[\frac{1}{8}\bar{\phi}\big(-\nabla^2 + m^2\big)^s\phi + \Big(V(\mathbf{x}) - \frac{\gamma_r^2|\mathbf{x}|^2}{2}\Big)|\phi|^2 + \frac{\beta}{2}|\phi|^4\Big]d\mathbf{x} + C_1 \le \mathcal{E}(\phi)$$
$$\le \int_{\mathbb{R}^d} \Big[\frac{7}{8}\bar{\phi}\big(-\nabla^2 + m^2\big)^s\phi + \Big(V(\mathbf{x}) + \frac{\gamma_r^2|\mathbf{x}|^2}{2}\Big)|\phi|^2 + \frac{\beta}{2}|\phi|^4\Big]d\mathbf{x} + C_2, \tag{3.3}$$

where $\gamma_r = \min\{\gamma_x, \gamma_y\}$, C_1 and C_2 are two constants that only depend on Ω, s, γ_r, d and μ.

Proof. (i) Using the Hardy–Littlewood–Sobolev (HLS) inequality, we have for the Coulomb-type interaction

$$\Big|\big\langle \Phi, \rho\big\rangle\Big| = \Big|\big\langle \mathcal{U}(\mathbf{x}) * \rho, \rho\big\rangle\Big| = \frac{1}{2^{d-1}\pi}\int_{\mathbb{R}^d}\int_{\mathbb{R}^d} \frac{\rho(\mathbf{x})\rho(\mathbf{y})}{|\mathbf{x}-\mathbf{y}|^\mu} d\mathbf{x}d\mathbf{y} \le c_{d,\mu}\|\rho\|_p^2 = c_{d,\mu}\|\phi\|_{2p}^4, \tag{3.4}$$

where $1 < p = \frac{2d}{2d-\mu} \le \frac{2d}{d+1} < 2$ and the constant $c_{d,\mu}$ depends only on d and μ. For the 3D case, i.e $d = 3$, let us introduce $\sigma = \frac{3-p}{2p}$. By the Hölder's inequality [49], we have

$$\Big|\big\langle \Phi, \rho\big\rangle\Big| \le c_{d,\mu}\Big(\|\phi\|_2^\sigma\ \|\phi\|_6^{1-\sigma}\Big)^4 = c_{d,\mu}\Big(\|\phi\|_6^2\Big)^{2(1-\sigma)}. \tag{3.5}$$

Now that $\mu \le d-1$, we have $0 < 2(1-\sigma) = \frac{\mu}{2} \le 1$. Thus, by Young's inequality [49], for $\forall\widetilde{\varepsilon} > 0$, we obtain

$$\Big(\|\phi\|_6^2\Big)^{2(1-\sigma)} \le 2(1-\sigma)\,\widetilde{\varepsilon}\,\|\phi\|_6^2 + (2\sigma-1)\widetilde{\varepsilon}^{\frac{2\sigma-2}{2\sigma-1}}. \tag{3.6}$$

Thus, together with the Sobolev inequality ([49], Chapter 8 Eq. (1)), i.e., there exists a constant C such that

$$\|\phi\|_6^2 \le C\|\nabla\phi\|^2, \tag{3.7}$$

we obtain

$$\Big|\big\langle \Phi, \rho\big\rangle\Big| \le 2(1-\sigma)\,c_{d,\mu}\,\widetilde{\varepsilon}\,C\,\|\nabla\phi\|^2 + (2\sigma-1)c_{d,\mu}\widetilde{\varepsilon}^{\frac{2\sigma-2}{2\sigma-1}} =: \varepsilon\,\|\nabla\phi\|^2 + C_\varepsilon. \tag{3.8}$$

Similarly, for the 2D case, let $q = \frac{4p}{2-p} > 2p > 2$ and $\sigma = \frac{q-2p}{p(q-2)}$. Then, one gets

$$\Big|\big\langle \Phi, \rho\big\rangle\Big| \le c_{d,\mu}\Big(\|\phi\|_2^\sigma\ \|\phi\|_q^{1-\sigma}\Big)^4 = c_{d,\mu}\Big(\|\phi\|_q^2\Big)^{2(1-\sigma)} \le \widetilde{\varepsilon}\,\|\phi\|_q^2 + \widetilde{C}_\varepsilon \le \varepsilon\,\|\nabla\phi\|_2^2 + C_\varepsilon. \tag{3.9}$$

(ii) Let $\gamma_r = \min\{\gamma_x, \gamma_y\}$. By Young's inequality and Plancherel's formula, we have

$$\Big|\Omega\int_{\mathbb{R}^d}\bar{\phi}L_z\phi\,d\mathbf{x}\Big| \le \int_{\mathbb{R}^d}\Big[\big|(\gamma_r x\bar{\phi})\,(\Omega\partial_y\phi/\gamma_r)\big| + \big|(\gamma_r y\bar{\phi})\,(\Omega\partial_x\phi/\gamma_r)\big|d\mathbf{x}\Big]$$

$$\le \frac{\gamma_r^2}{2}\int_{\mathbb{R}^d}|\mathbf{x}|^2|\phi|^2d\mathbf{x} + \frac{\Omega^2}{2\gamma_r^2}\int_{\mathbb{R}^d}|\nabla\phi|^2\,d\mathbf{x} = \frac{\gamma_r^2}{2}\int_{\mathbb{R}^d}|\mathbf{x}|^2|\phi|^2d\mathbf{x} + \frac{\Omega^2}{2\gamma_r^2(2\pi)^d}\int_{\mathbb{R}^d}|\mathbf{k}|^2|\widehat{\phi}|^2d\mathbf{k}$$

$$\le \frac{\gamma_r^2}{2}\int_{\mathbb{R}^d}|\mathbf{x}|^2|\phi|^2d\mathbf{x} + \frac{\Omega^2}{2\gamma_r^2(2\pi)^d}\int_{\mathbb{R}^d}\Big[\frac{\gamma_r^2(|\mathbf{k}|^2+m^2)^s}{2\Omega^2} + \Big(\frac{\gamma_r^2}{2\Omega^2}\Big)^{\frac{1}{1-s}}\Big]|\widehat{\phi}|^2\,d\mathbf{k} - \frac{\Omega^2m^2}{2\gamma_r^2}$$

$$\le \frac{\gamma_r^2}{2}\int_{\mathbb{R}^d}|\mathbf{x}|^2|\phi|^2d\mathbf{x} + \frac{1}{4}\int_{\mathbb{R}^d}\bar{\phi}\big(-\nabla^2+m^2\big)^s\phi\,d\mathbf{x} + C. \tag{3.10}$$

Similarly, for the Coulomb-type nonlocal interaction, together with (3.2), we have

$$\Big|\frac{\lambda}{2}\langle\Phi,\rho\rangle\Big| \le \widetilde{\varepsilon}\|\nabla\phi\|_2^2 + \widetilde{C}_\varepsilon = \frac{\widetilde{\varepsilon}}{(2\pi)^d}\int_{\mathbb{R}^d}|\mathbf{k}|^2\,|\widehat{\phi}|^2\,d\mathbf{k} + \widetilde{C}_\varepsilon \le \frac{1}{(2\pi)^d}\int_{\mathbb{R}^d}\Big[\frac{1}{8}(|\mathbf{k}|^2+m^2)^s + C\Big]|\widehat{\phi}|^2\,d\mathbf{k}$$

$$= \frac{1}{8}\int_{\mathbb{R}^d}\bar{\phi}\big(-\nabla^2+m^2\big)^s\phi\,d\mathbf{x} + C. \tag{3.11}$$

Therefore, the inequality (3.3) follows from (3.10) and (3.11). □

Theorem 3.1. *If $V(\mathbf{x})$ is a trapping harmonic potential defined in (1.4), then the following properties hold.*

(i) *If $s>1$ and $\beta\ge 0$, then there exists a ground state of the FNLSE for all $\Omega>0$ if one of the following conditions holds:*
(A) *$\mathcal{U}(\mathbf{x})$ reads as Coulomb-type. (B) For 3D DDI: $-\beta/2\le\lambda\le\beta$.*
(C) *For 2D DDI: (c1) $\lambda=0$. (c2) $\lambda>0$ and $n_3=0$. (c3) $\lambda<0$ and $n_3^2\ge\frac{1}{2}$.*

(ii) *If $\Omega=0$, $\beta\ge 0$, then the ground state exists for all $s>0$ if one of the following conditions holds:*
(1) *$\mathcal{U}(\mathbf{x})$ reads as Coulomb-type and $\lambda\ge 0$.(2) (B) or (C) in (i) holds.*

(iii) *If $0<s<1$, there exists no ground state if one of the following conditions holds:*
(A) *$\forall\,\Omega>0$, $\lambda=0$. (B) $\forall\,\Omega>0$, $\mathcal{U}(\mathbf{x})$ is a Coulomb-type interaction or a 3D DDI.*
(C) *$\mathcal{U}(\mathbf{x})$ is the 2D DDI, $\forall\,\Omega>\Omega_0=c|\lambda|^{\frac{2}{5}}$ with $c=\big(\frac{(2\pi^2+1)^4\gamma^6}{48e\pi^9}\big)^{\frac{1}{5}}$ (≈ 0.54 for $\gamma=1$). Here, $\gamma=\max\{\gamma_x,\gamma_y\}$.*

Proof. (i) For the Coulomb-type interaction, it is clear by Lemma 3.1 that the energy functional $\mathcal{E}$ is bounded below, coercive and weakly lower semi-continuous on S. Hence, (A) follows. For the DDI, the proof is similar as those for the non-fractional case [9,10] by noticing (3.10). Similar arguments lead to (ii).

(iii) Denote $\gamma=\max\{\gamma_x,\gamma_y\}$. In 2D, we choose the function

$$\phi_n(\mathbf{x}) = \mathcal{F}^{-1}(\widehat{\phi}_n)(\mathbf{x}), \quad \text{with} \quad \widehat{\phi}_n(\mathbf{k}) = \mathcal{F}(\phi_n)(\mathbf{k}) = \Big(4\pi\varepsilon^{n+1}\Big)^{1/2}(n!)^{-1/2}\exp(-\varepsilon|\mathbf{k}|^2/2)|\mathbf{k}|^n e^{in\theta}. \tag{3.12}$$

By Plancherel's formula, it is easy to check that $\|\phi_n\|_2=\frac{1}{2\pi}\|\widehat{\phi}_n\|_2=1$, and thus $\phi_n\in S$. Let $\rho_n=|\phi_n|^2$. By Young's inequality and Cauchy–Schwarz inequality, we obtain

$$\mathcal{E}_1(\phi_n) =: \mathcal{E}_{\rm kin}(\phi_n)+\mathcal{E}_{\rm pot}(\phi_n)+\mathcal{E}_{\rm rot}(\phi_n)$$

$$\le \frac{1}{4\pi^2}\Big[\frac{1}{2}\langle\big(|\mathbf{k}|^2+m^2\big)^s\widehat{\phi}_n,\widehat{\phi}_n\rangle - \frac{\gamma^2}{2}\langle\Delta\widehat{\phi}_n,\widehat{\phi}_n\rangle - i\Omega\langle\widehat{J}_{z_k}\widehat{\phi}_n,\widehat{\phi}_n\rangle\Big]$$

$$\le \frac{e^{m^2\varepsilon}}{2\varepsilon^s}\frac{\Gamma(n+1+s)}{\Gamma(n+1)} + \Big(\frac{\varepsilon\gamma^2}{2}-\Omega\Big)n + \frac{\varepsilon\gamma^2}{2}, \tag{3.13}$$

$$|\mathcal{E}_{\rm int}(\phi_n)| = \frac{|\beta|}{2}\|\rho_n\|_2^2 = \frac{|\beta|}{2(2\pi)^6}\|\widehat{\phi}_n*\widehat{\phi_n^*}\|_2^2 \le \frac{|\beta|}{2(2\pi)^4}\Big(\frac{1}{(2\pi)^2}\|\widehat{\phi}_n\|_2^2\Big)\|\widehat{\phi}_n\|_1^2$$

$$= \frac{|\beta|}{2(2\pi)^4}\|\widehat{\phi}_n\|_1^2 = \frac{|\beta|}{2\pi\varepsilon}\,\frac{2^n\big(\Gamma(n/2+1)\big)^2}{\Gamma(n+1)}. \tag{3.14}$$

Furthermore, we compute the nonlocal interaction energy $\mathcal{E}_{\rm non}(\phi_n)$. For the Coulomb-type interaction, by using the HLS inequality (3.4) and the Hölder's inequality, we obtain

$$\left|\mathcal{E}_{\rm non}(\phi_n)\right| \le \frac{c_\mu|\lambda|}{2}\|\rho_n\|_p^2 \le \widetilde{c}_\mu\|\rho_n\|_1^{2-\mu}\|\rho_n\|_2^{\mu} \le \widetilde{c}_\mu\left[\frac{1}{\pi\varepsilon}\,\frac{2^n\big(\Gamma(n/2+1)\big)^2}{\Gamma(n+1)}\right]^{\mu/2}, \tag{3.15}$$

where $p=\frac{4}{4-\mu}$, $0<\mu\le 1$, and $\widetilde{c}_\mu$ depends only on μ and λ. Together with the Stirling's formula

$$\Gamma(x+1)\sim\sqrt{2\pi x}\left(\frac{x}{e}\right)^x, \text{ when } \quad x\to\infty, \tag{3.16}$$

one gets

$$|\mathcal{E}_{\rm int}(\phi_n)|\sim\sqrt{n}, \qquad |\mathcal{E}_{\rm non}(\phi_n)|\sim\sqrt{n}, \qquad n\to\infty. \tag{3.17}$$

Let $\varepsilon<\frac{2\Omega}{\gamma^2}$, $\forall\,\Omega>0$ and $s<1$, we then prove that

$$\begin{aligned}\limsup_{n\to\infty}\mathcal{E}(\phi_n) &\le \limsup_{n\to\infty}\left[\mathcal{E}_1(\phi_n)+|\mathcal{E}_{\rm int}(\phi_n)|+\mathcal{E}_{\rm non}(\phi_n)\right]\\ &\le \limsup_{n\to\infty}\left[\frac{c_2n^s}{2\varepsilon^s}+\left(\frac{\varepsilon\gamma^2}{2}-\Omega\right)n+c_1\sqrt{n}+c_0\right]=-\infty,\end{aligned} \tag{3.18}$$

which implies the nonexistence of the ground states. Thus (B) follows. (A) also results by simply setting $c_1=0$ in (3.18). For the 2D DDI, we have

$$\left|\mathcal{E}_{\rm non}(\phi_n)\right| = \frac{|\lambda|}{8\pi^2}\left|\langle\widehat{\mathcal{U}}\widehat{\rho_n},\widehat{\rho_n}\rangle\right| \le \frac{|\lambda|}{8\pi^2}\left\langle\frac{3(|\mathbf{k}\cdot\mathbf{n}_\perp|^2+n_3^2|\mathbf{k}|^2)}{2|\mathbf{k}|}\widehat{\rho_n},\widehat{\rho_n}\right\rangle \le \frac{3|\lambda|}{16\pi^2}\langle|\mathbf{k}|\,\widehat{\rho_n},\widehat{\rho_n}\rangle. \tag{3.19}$$

By the generalized Minkowski inequality, we obtain

$$\begin{aligned}4\pi^2\Big(\langle|\mathbf{k}|\,\widehat{\rho_n},\widehat{\rho_n}\rangle\Big)^{\frac12} &= \left[\int_{\mathbb{R}^2}|\mathbf{k}|\left|\int_{\mathbb{R}^2}\widehat{\phi_n}(\mathbf{k}-\boldsymbol{\xi})\widehat{\bar\phi_n}(\boldsymbol{\xi})d\boldsymbol{\xi}\right|^2d\mathbf{k}\right]^{\frac12} \le \int_{\mathbb{R}^2}\left[\int_{\mathbb{R}^2}|\mathbf{k}|\left|\widehat{\phi_n}(\mathbf{k}-\boldsymbol{\xi})\right|^2\left|\widehat{\bar\phi_n}(\boldsymbol{\xi})\right|^2d\mathbf{k}\right]^{\frac12}d\boldsymbol{\xi}\\ &= \int_{\mathbb{R}^2}\left|\widehat{\bar\phi_n}(\boldsymbol{\xi})\right|\left[\int_{\mathbb{R}^2}|\mathbf{k}-\boldsymbol{\xi}|\left|\widehat{\phi_n}(\mathbf{k})\right|^2d\mathbf{k}\right]^{\frac12}d\boldsymbol{\xi} \le \int_{\mathbb{R}^2}\left|\widehat{\bar\phi_n}(\boldsymbol{\xi})\right|\left[\int_{\mathbb{R}^2}(|\mathbf{k}|+|\boldsymbol{\xi}|)\left|\widehat{\phi_n}(\mathbf{k})\right|^2d\mathbf{k}\right]^{\frac12}d\boldsymbol{\xi}\\ &\le \int_{\mathbb{R}^2}\left|\widehat{\bar\phi_n}(\boldsymbol{\xi})\right|\left[\sqrt{|\boldsymbol{\xi}|}+\left(\int_{\mathbb{R}^2}|\mathbf{k}|\left|\widehat{\phi_n}(\mathbf{k})\right|^2d\mathbf{k}\right)^{\frac12}\right]d\boldsymbol{\xi} = \left(\left\|\sqrt{|\mathbf{k}|}\,\widehat{\phi_n}\right\|_1+\left\|\widehat{\phi_n}\right\|_1\left\|\sqrt{|\mathbf{k}|}\,\widehat{\phi_n}\right\|_2\right)\\ &= \frac{\pi^{\frac12}2^{\frac{n}{2}+\frac94}}{\varepsilon^{\frac34}}\,\frac{\Gamma(\frac{n}{2}+\frac54)}{\sqrt{\Gamma(n+1)}}+\frac{\pi^{\frac52}2^{\frac{n}{2}+3}}{\varepsilon^{\frac34}}\,\frac{\sqrt{\Gamma(n+\frac32)}\,\Gamma(\frac{n}{2}+1)}{\Gamma(n+1)}.\end{aligned} \tag{3.20}$$

Again, by the Stirling's formula (3.16), we show that

$$|\mathcal{E}_{\rm non}(\phi_n)| \precsim \frac{c_3|\lambda|}{\varepsilon^{3/2}}n, \qquad n\to\infty, \tag{3.21}$$

where $c_3=\frac{3\sqrt{2}(2\pi^2+1)^2}{32\pi\sqrt[4]{e\pi}}$. Let us set $\varepsilon=\left(3c_3|\lambda|/\gamma^2\right)^{\frac25}$ and $\Omega>\Omega_0=\left(\frac{(2\pi^2+1)^4\gamma^6}{48e\pi^9}\right)^{\frac15}|\lambda|^{\frac25}$. It follows that

$$\limsup_{n\to\infty}\mathcal{E}(\phi_n)\le\limsup_{n\to\infty}\left[\frac{c_2n^s}{2\varepsilon^s}+\left(\frac{\varepsilon\gamma^2}{2}+\frac{c_3}{\varepsilon^{\frac32}}-\Omega\right)n+c_1\sqrt{n}+c_0\right]=-\infty,$$

leading to the nonexistence of the ground states. Hence (C) follows.

In 3D, we choose the sequence

$$\phi_n^{\rm 3D}(\mathbf{x})=\phi_n(x,y)\phi(z), \tag{3.22}$$

where $\phi(z)=\left(\frac{\gamma_z}{\pi}\right)^{1/4}\exp\{-\frac{\gamma_z z^2}{2}\}$ and $\phi_n(x,y)=\mathcal{F}^{-1}(\widehat{\phi_n}(\mathbf{k}))$, with $\widehat{\phi_n}(\mathbf{k})$ reading as (3.12). Then, the argument proceeds similarly as those in 2D for the 3D Coulomb potential. As for the 3D DDI, noticing that

$$|\mathcal{E}_{\rm non}(\phi_n^{\rm 3D})| \le \frac{3|\lambda|}{2}\|\phi_n^{\rm 3D}\|_4^4 = \frac{3|\lambda|\sqrt{\gamma_z}}{2\sqrt{2\pi}}\|\phi_n\|_4^4 = \frac{3|\lambda|\sqrt{\gamma_z}}{2\sqrt{2\pi}}\|\rho_n\|_2^2, \tag{3.23}$$

the left argument proceeds similarly as those in 2D from (3.14). □

Remark 3.1. For the 2D DDI, one open question concerns the plausible fact that (iii)(C) in Theorem 3.1 maybe hold for $\forall\,\Omega_0 > 0$. The proof presented here does not seem to be directly applicable for this conjecture.

Remark 3.2. It might be interesting to understand the existence/non-existence and the uniqueness of the ground states for the more general FNLSE

$$i\partial_t\psi = \left[\frac{1}{2}(-\nabla^2+m^2)^s + \frac{1}{2}\gamma_r^2|\mathbf{x}|^p + \beta|\psi|^q + \lambda\Phi - \Omega L_z\right]\psi, \tag{3.24}$$

where the constants β and λ can be positive or negative and the powers p and q are real-valued positive constants. We leave it as an open problem for some future studies.

3.2. Numerical method

For a constant time step Δt, we introduce the discrete times $t_n = n\Delta t$ for $n = 0, 1, 2, \ldots$ The gradient flow with discrete normalization (GFDN) method reads as

$$\partial_t\phi(\mathbf{x},t) = -\left[\frac{1}{2}(-\nabla^2+m^2)^s + V(\mathbf{x}) + \beta|\phi|^2 + \lambda\,\Phi(\mathbf{x},t) - \Omega L_z\right]\phi(\mathbf{x},t), \tag{3.25}$$

$$\Phi(\mathbf{x},t) = \left(\mathcal{U} * |\phi|^2\right)(\mathbf{x},t), \qquad \mathbf{x}\in\mathbb{R}^d, \quad t_n \le t < t_{n+1}, \tag{3.26}$$

$$\phi(\mathbf{x},t_{n+1}) = \frac{\phi(\mathbf{x},t_{n+1}^-)}{\|\phi(\mathbf{x},t_{n+1}^-)\|_2}, \qquad \mathbf{x}\in\mathbb{R}^d, \quad n\ge 0, \tag{3.27}$$

with the initial data

$$\phi(\mathbf{x},0) = \phi_0(\mathbf{x}), \qquad \mathbf{x}\in\mathbb{R}^d, \qquad \text{with} \qquad \|\phi_0\|_2 = 1. \tag{3.28}$$

Let $\phi^n(\mathbf{x})$ and $\Phi^n(\mathbf{x})$ be the approximations of $\phi(\mathbf{x},t_n)$ and $\Phi(\mathbf{x},t_n)$, respectively. The above GFDN is usually discretized in time *via* the semi-implicit backward Euler method [4,13,16,60]

$$\frac{\phi^{(1)}(\mathbf{x}) - \phi^n(\mathbf{x})}{\Delta t} = -\left[\frac{1}{2}(-\nabla^2+m^2)^s + V(\mathbf{x}) + \beta|\phi^n|^2 + \lambda\,\Phi^n(\mathbf{x}) - \Omega L_z\right]\phi^{(1)}(\mathbf{x}), \tag{3.29}$$

$$\Phi^n(\mathbf{x}) = \left(\mathcal{U} * |\phi^n|^2\right)(\mathbf{x}), \qquad \mathbf{x}\in\mathbb{R}^d, \tag{3.30}$$

$$\phi^{n+1}(\mathbf{x}) = \frac{\phi^{(1)}(\mathbf{x})}{\|\phi^{(1)}(\mathbf{x})\|_2}, \qquad \mathbf{x}\in\mathbb{R}^d, \quad n\ge 0. \tag{3.31}$$

The ground states decay exponentially fast due to the trapping potential. Therefore, in practical computations, we first truncate the whole space to a bounded rectangular domain and impose periodic boundary conditions. Then, we discretize the equation (3.29) *via* the Fourier pseudo-spectral method in space and evaluate the nonlocal interaction $\Phi^n(\mathbf{x})$ by the GauSum solver. The full discretized scheme of system (3.29)–(3.31) can then be solved by a fixed-point iteration or a preconditioned Krylov subspace solver with a similar preconditioner as those in [4]. Let us define the operators

$$A^{\rm BE,n} := \frac{I}{\Delta t} + \frac{1}{2}(-\nabla^2+m^2)^s + V(\mathbf{x}) + \beta|\phi^n|^2 + \lambda\,\Phi^n(\mathbf{x}) - \Omega L_z, \tag{3.32}$$

$$P_{\Delta}^{\rm BE} = \left[\frac{I}{\Delta t} + \frac{1}{2}(-\nabla^2+m^2)^s\right]^{-1}, \qquad A_{\rm TF}^{\rm BE,n} = V(\mathbf{x}) + \beta|\phi^n|^2 + \lambda\,\Phi^n(\mathbf{x}) - \Omega L_z, \tag{3.33}$$

$$P_{\rm TF}^{\rm BE,n} = \left[\frac{I}{\Delta t} + V(\mathbf{x}) + \beta|\phi^n|^2 + \lambda\,\Phi^n(\mathbf{x})\right]^{-1}, \qquad A_{\Delta,\Omega}^{\rm BE,n} = \frac{1}{2}(-\nabla^2+m^2)^s - \Omega L_z. \tag{3.34}$$

Moreover, we denote by $\mathbb{I}$, $\mathbb{A}^{\rm BE,n}$, $\mathbb{P}_{\Delta}^{\rm BE}$, $\mathbb{A}_{\rm TF}^{\rm BE,n}$, $\mathbb{P}_{\rm TF}^{\rm BE,n}$, $\mathbb{A}_{\Delta,\Omega}^{\rm BE,n}$ the discretized versions of the above operators, and by $\boldsymbol{\phi}^{(1)}$ and $\boldsymbol{\phi}^n$ the discretization of $\phi^{(1)}$ and ϕ^n through the Fourier pseudo-spectral approximation. Then, the finite-dimensional linear system corresponding to (3.29)–(3.31) reads as

$$\mathbb{A}^{\rm BE,n}\boldsymbol{\phi}^{(1)} = \boldsymbol{b}^n := \boldsymbol{\phi}^n/\Delta t. \tag{3.35}$$

Two preconditioned versions of the linear system are the following

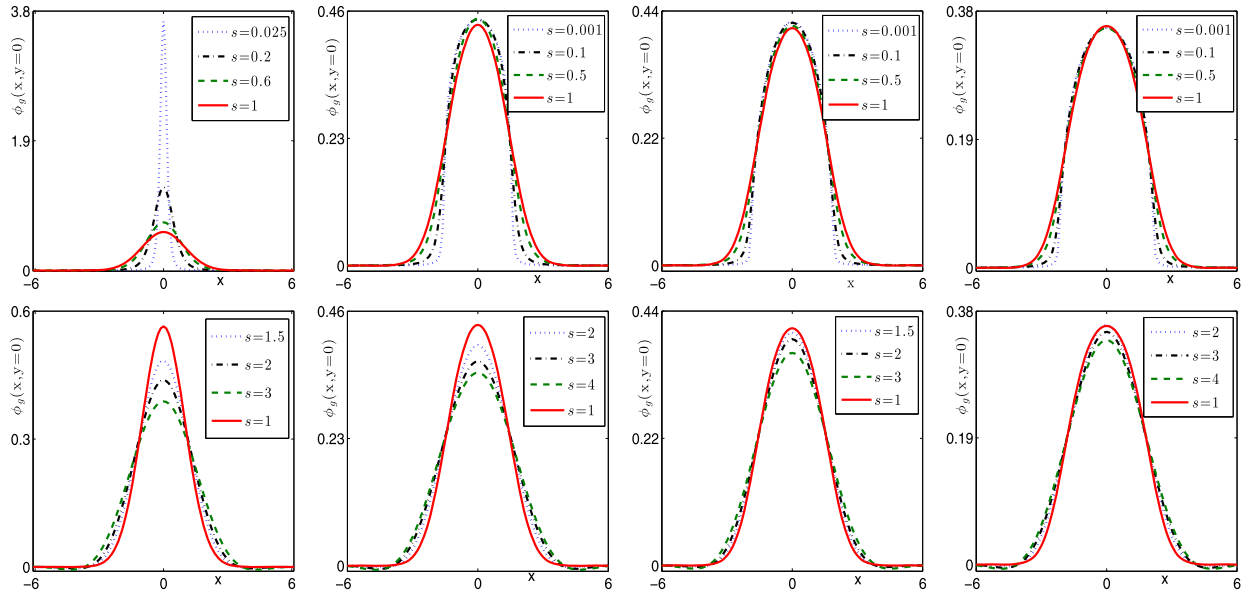

Fig. 1. Slice plots of $\phi_g(x,0)$ for **Cases I–IV** (from left to right) for subdispersion $s \le 1$ (top row) and superdispersion $s \ge 1$ (bottom) in Example 3.1.

$$\left(\mathbb{I} + \mathbb{P}_{\Delta}^{\mathrm{BE}} \mathbb{A}_{\mathrm{TF}}^{\mathrm{BE,n}}\right) \boldsymbol{\phi}^{(1)} = \mathbb{P}_{\Delta}^{\mathrm{BE}} \boldsymbol{b}^n, \qquad \text{or} \qquad \left(\mathbb{I} + \mathbb{P}_{\mathrm{TF}}^{\mathrm{BE,n}} \mathbb{A}_{\Delta,\Omega}^{\mathrm{BE,n}}\right) \boldsymbol{\phi}^{(1)} = \mathbb{P}_{\mathrm{TF}}^{\mathrm{BE,n}} \boldsymbol{b}^n. \tag{3.36}$$

We refer the reader to [4] for more details and omit them here for brevity. Like in the standard case [4,7], the most efficient solver uses the first preconditioned system (left) in (3.36) based on $\mathbb{P}_{\Delta}^{\mathrm{BE}}$. In particular, the acceleration of the convergence of the Krylov subspace solver (BiCGStab) is visible when Ω, β and λ are large. In practice, we use this preconditioned solver in subsection 3.3.

3.3. Numerical results

In this subsection, we report some numerical results concerning the ground states of (1.1)–(1.2) computed by the *GF-GauSum* solver. To this end, unless stated, we fix $m = 0$ and $d = 2$. The computational domain, mesh sizes and time step are respectively chosen as $\mathbf{B} = [-32, 32] \times [-32, 32]$, $h_x = h_y = \frac{1}{8}$ and $\Delta t = 10^{-3}$. The trapping potential $V(\mathbf{x})$ is chosen as (1.4) with $\gamma_x = \gamma_y = 1$. The nonlocal interaction is of Coulomb-type with $\mu = 1$. The initial guess $\phi_0(\mathbf{x})$ is chosen as

$$\phi_0(\mathbf{x}) = \frac{(1-\Omega)\phi_{\mathrm{ho}}(\mathbf{x}) + \Omega\phi_{\mathrm{ho}}^{v}(\mathbf{x})}{\|(1-\Omega)\phi_{\mathrm{ho}}(\mathbf{x}) + \Omega\phi_{\mathrm{ho}}^{v}(\mathbf{x})\|}, \quad \text{with } \phi_{\mathrm{ho}}(\mathbf{x}) = \frac{1}{\sqrt{\pi}} e^{-\frac{|\mathbf{x}|^2}{2}}, \ \phi_{\mathrm{ho}}^{v}(\mathbf{x}) = \frac{x+iy}{\sqrt{\pi}} e^{-\frac{|\mathbf{x}|^2}{2}}, \ \mathbf{x} \in \mathbf{B}. \tag{3.37}$$

The ground state $\phi_g(\mathbf{x})$ is reached when the stopping criterion holds: $\|\phi^n(\mathbf{x}) - \phi^{n+1}(\mathbf{x})\|_\infty \le \varepsilon_0 \Delta t$. In the computations, we choose the accuracy parameter $\varepsilon_0 = 10^{-9}$.

Example 3.1 *(Non-rotating FNLSE).* Here, we impose $\Omega = 0$. We study the ground states of the following four cases:

- **Case I**. Linear case, i.e. $\beta = \lambda = 0$.
- **Case II**. Purely long-range interaction, i.e. $\beta = 0$ and $\lambda = 10$.
- **Case III**. Purely short-range interaction, i.e. $\beta = 10$ and $\lambda = 0$.
- **Case IV**. Both long-range and short-range interactions, i.e. $\lambda = \beta = 10$.

Fig. 1 shows the slice plots of the ground states along the x-axis, i.e. $\phi_g(x,0)$, for different fractional orders s of the FNLSE.

Example 3.2 *(Non-rotating FNLSE with harmonic + optical lattice potential).* Here, we choose $\Omega = 0$. We consider the ground states of the FNLSE in a harmonic plus optical lattice potential with different parameters. To this end, we let $\lambda = 64$ and $\beta = 0$ and choose the potential as

$$V(x,y) = \frac{x^2+y^2}{2} + 10\big(\sin^2(\pi x) + \sin^2(\pi y)\big).$$

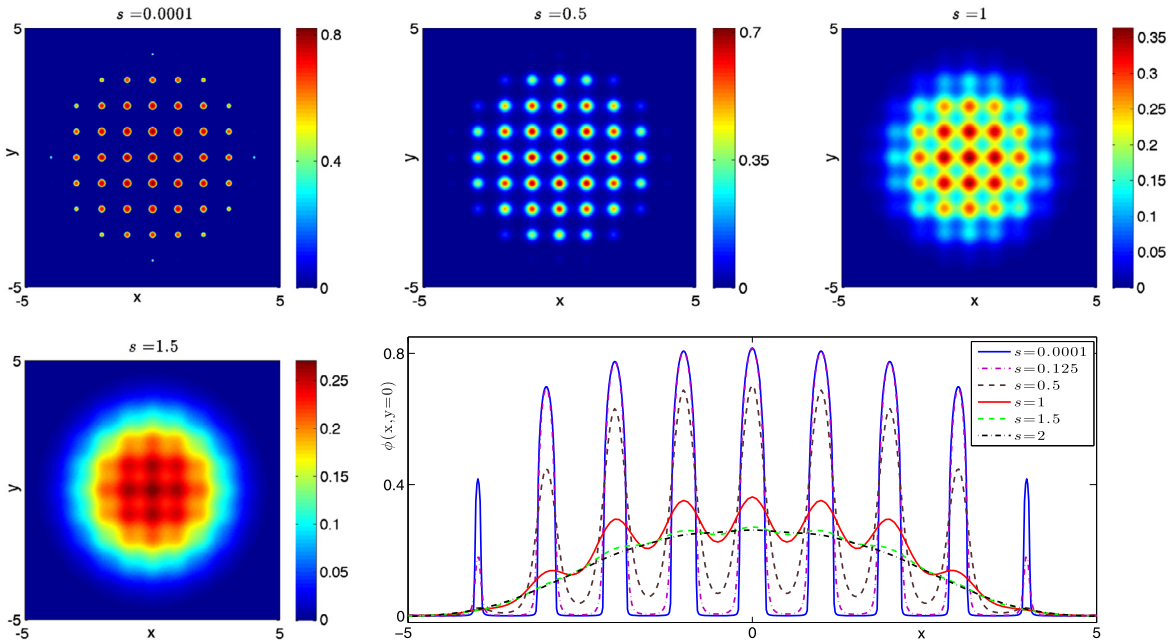

Fig. 2. Contour plots of the density of the ground state $\phi_g(x, y)$ and the slice plot of $\phi_g(x, y = 0)$ in Example 3.2.

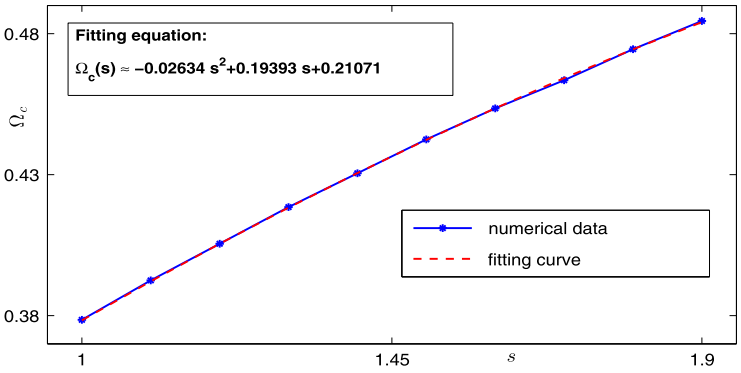

Fig. 3. Critical rotating frequency vs. the fractional order s in Example 3.3.

The spatial mesh sizes are chosen as $h_x = h_y = \frac{1}{32}$ in this case. Fig. 2 shows the contour plot of the ground state density $\rho_g := |\phi_g(\mathbf{x})|^2$ and the slice plot of $\phi_g(x, 0)$ with different fractional orders s.

From Figs. 1–2 and additional results not shown here, we can conclude that (i) The ground states become more peaked and narrower as the fractional order s tends smaller, which corresponds to subdispersion. (ii) A large fractional order helps in smoothing out the density profile (cf. Fig. 2) for the superdispersion case. (iii) The repulsive local/nonlocal interactions suppress the "focus" or "homogenization" effect as the dispersive order s tends smaller or larger. In other words, the repulsive nonlinear interaction helps to stabilize the ground states. (iv) When β and/or λ are/is large, the nonlinear interaction dominates and the dispersive effect can be neglected.

Example 3.3 *(Rotating FGPE).* In this example, we present the ground states of the rotating FGPE with only local nonlinear interaction, i.e. $\lambda = 0$. We fix $\beta = 100$.

We propose to numerically study the dependence of the first critical rotating velocity Ω_c to create a vortex with respect to the fractional order s. Fig. 3 shows this relation derived by a linear regression

$$\Omega_c(s) \approx -0.02634\, s^2 + 0.19393\, s + 0.21071. \tag{3.38}$$

Fig. 4 displays the contour plots of the ground state density $\rho_g =: |\phi_g|^2$ for different Ω but with $s = 1.2$ (superdispersion), while Fig. 5 shows those for different s but with $\Omega = 1.35$.

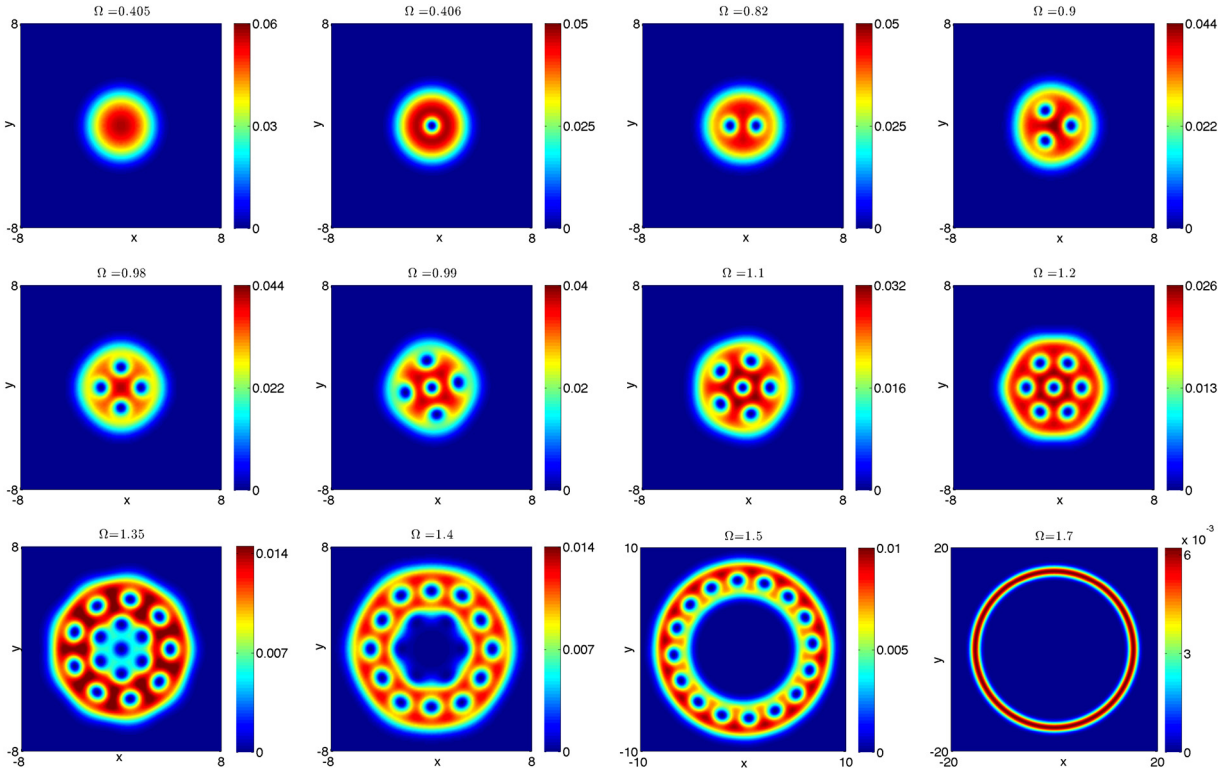

Fig. 4. Contour plots of the density $|\phi_g(\mathbf{x})|^2$ in Example 3.3: $s = 1.2$ (superdispersion) is fixed and Ω varies.

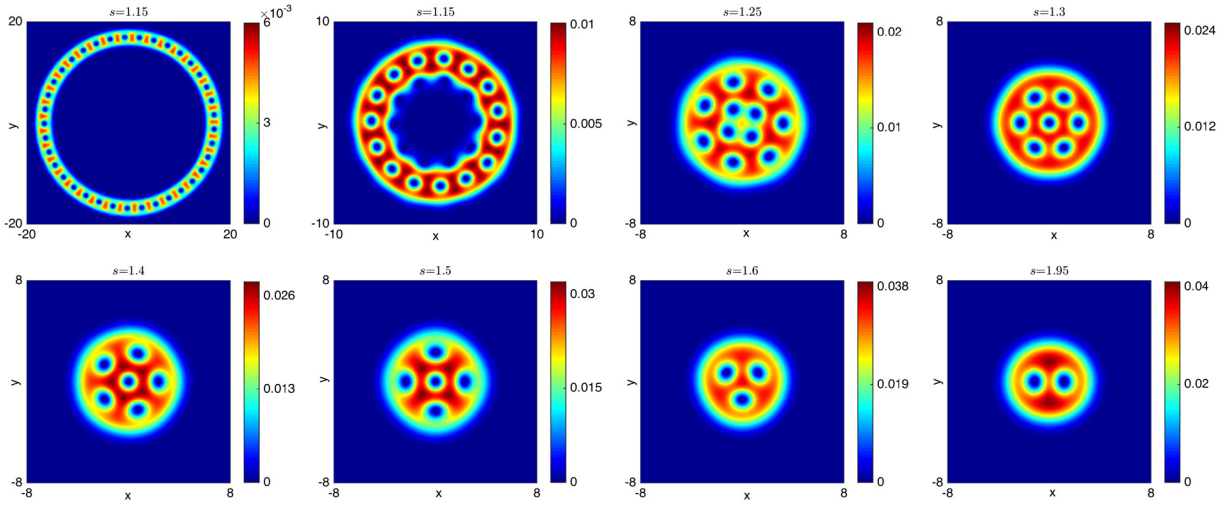

Fig. 5. Contour plots of the density $|\phi_g(\mathbf{x})|^2$ in Example 3.3: $\Omega = 1.35$ is fixed and s varies.

From Figs. 3–5 and additional results not shown here, we can conclude that (i) The first critical rotating velocity Ω_c depends almost linearly on s. (ii) For the superdispersion case, i.e. $s > 1$, the ground states exist for all velocities Ω. As Ω increases, the ground states will undergo three phase transitions (similar to the non-fractional GPE with quartic order trapping potential), i.e., from Gaussian-type to one-vortex profile, from vortex lattice to vortex-lattice with a hole at the center and then to a giant vortex. (iii) For fixed Ω, the vortex lattice pattern depends crucially on s. As s changes, the ground states will undergo similar phase transitions as in the case where s is fixed and Ω varies. It would be interesting to study how these critical rotating frequencies for the transitions depend on s and Ω as well as how they compare with those in the case of the standard GPE.

4. Dynamics computation: properties, numerical scheme and simulations

In this section, we first present analogous dynamical laws for some commonly used quantities in the classical rotating GPE. Then, we extend the rotating Lagrangian coordinates transform [14] to the FGPE. In the rotating Lagrangian coordinates, the rotation term vanishes, giving rise to a time-dependent potential. Based on the new FNLSE, we propose a time-splitting Fourier pseudo-spectral method incorporated with the GauSum solver to simulate the dynamics.

4.1. Dynamical properties

Here we study the dynamical properties of the mass, energy, angular momentum expectation and center of mass [14]. The dynamical laws can be used as benchmarks to test the numerical methods and are briefly listed here. For details, one can either refer to appendices or to [55] for analogous proofs to their non-fractional counterparts.

Mass and energy. The FNLSE (1.1)–(1.2) conserves the mass (1.6) and the energy (1.7), i.e.

$$\mathcal{N}(t) = \mathcal{N}(t=0), \qquad \mathcal{E}(t) = \mathcal{E}(t=0). \tag{4.1}$$

Proof. It is straightforward to prove in a similar way as their non-fractional counterparts [55] by using the Plancherel's formula. □

Angular momentum expectation. The *angular momentum expectation* is defined as

$$\langle L_z \rangle(t) = \int_{\mathbb{R}^d} \bar{\psi}(\mathbf{x},t) L_z \psi(\mathbf{x},t)\, d\mathbf{x}, \qquad t \geq 0. \tag{4.2}$$

Lemma 4.1. *The angular momentum expectation $\langle L_z \rangle(t)$ satisfies the following equation*

$$\frac{d}{dt}\langle L_z \rangle(t) = \int_{\mathbb{R}^d} |\psi|^2 (y\partial_x - x\partial_y)\big(V(\mathbf{x}) + \lambda\Phi(\mathbf{x},t)\big) d\mathbf{x}. \tag{4.3}$$

This implies that the angular momentum expectation is conserved, i.e.

$$\langle L_z \rangle(t) = \langle L_z \rangle(0), \qquad t \geq 0, \tag{4.4}$$

when $V(\mathbf{x})$ is radially/cylindrically symmetric in 2D/3D and one of the following conditions holds: (i) $\lambda = 0$, (ii) $\lambda \neq 0$, $\Phi(\mathbf{x})$ is the Coulomb potential or (iii) $\lambda \neq 0$, $\Phi(\mathbf{x})$ is the dipole potential with dipole axis parallel to the z-axis, i.e. $\mathbf{n} = (0,0,\pm 1)^T$.

Proof. Details of the proof are given in Appendix A. □

Center of mass. The center of mass is defined by

$$\mathbf{x}_c(t) = \int_{\mathbb{R}^d} \mathbf{x}\, |\psi(\mathbf{x},t)|^2 d\mathbf{x} = \langle \mathbf{x}\psi, \psi \rangle. \tag{4.5}$$

Lemma 4.2. *The center of mass $\mathbf{x}_c(t)$ satisfies the following equations, for $0 < s \leq 1$ (subdispersion),*

$$\dot{\mathbf{x}}_c - \Omega J \mathbf{x}_c = i\big\langle G * \psi, \nabla\psi \big\rangle, \tag{4.6}$$

$$\ddot{\mathbf{x}}_c - 2\Omega J \dot{\mathbf{x}}_c + \Omega^2 J^2 \mathbf{x}_c = 2\mathrm{Re}\Big(\big\langle G * (\mathcal{V}\psi), \nabla\psi \big\rangle\Big). \tag{4.7}$$

Here, we set $\mathcal{V}(\mathbf{x}, |\psi|) = V(\mathbf{x}) + \beta|\psi|^2 + \lambda\Phi(\mathbf{x},t)$, and

$$J = \begin{pmatrix} 0 & 1 \\ -1 & 0 \end{pmatrix}, \quad \text{for} \quad d=2, \qquad J = \begin{pmatrix} 0 & 1 & 0 \\ -1 & 0 & 0 \\ 0 & 0 & 0 \end{pmatrix}, \quad \text{for} \quad d=3. \tag{4.8}$$

The convolution kernel $G(\mathbf{x})$ reads as

$$G(\mathbf{x}) = \begin{cases} \delta(\mathbf{x}), & s = 1, \\ \dfrac{2^{s-d/2}s}{\Gamma(1-s)\,\pi^{d/2}} \left(\dfrac{m}{|\mathbf{x}|}\right)^{\frac{d}{2}+s-1} K_{\frac{d}{2}+s-1}\big(m|\mathbf{x}|\big), & 0 < s < 1, \end{cases} \tag{4.9}$$

where $\delta(\mathbf{x})$ is the Dirac delta function and $K_\nu(z)$, the modified Bessel function of the second-kind and order ν, is given explicitly as follows

$$K_\nu(z) = \frac{(2z)^\nu \Gamma(\nu+\frac{1}{2})}{\sqrt{\pi}} \int_0^\infty \frac{\cos(t)}{(t^2+z^2)^{\nu+\frac{1}{2}}} dt. \tag{4.10}$$

Proof. A detailed proof is reported in Appendix B. □

Remark 4.1. If $s=1$, $V(\mathbf{x})$ is the harmonic potential (1.4) and $\Phi(\mathbf{x})$ is the Coulomb potential or DDI with $\mathbf{n}=(0,0,1)^T$, then (4.7) reduces to [14,44]

$$\ddot{\mathbf{x}}_c - 2\Omega J\dot{\mathbf{x}}_c + (\Omega^2 J^2 + \Lambda_d)\mathbf{x}_c = \mathbf{0}, \tag{4.11}$$

where

$$\Lambda_d = \begin{pmatrix} \gamma_x^2 & 0 \\ 0 & \gamma_y^2 \end{pmatrix}, \quad \text{for} \quad d=2, \qquad \Lambda_d = \begin{pmatrix} \Lambda_2 & \mathbf{0} \\ \mathbf{0} & \gamma_z^2 \end{pmatrix}, \quad \text{for} \quad d=3. \tag{4.12}$$

In [44], the authors derived a dynamical law for the center of mass for the FNLSE with $s \in (\frac{1}{2}, 1]$ and a harmonic trapping potential. Compared with their results, the dynamical laws (4.6)–(4.7) are simpler and hold for a general potential $V(\mathbf{x})$ as well as for the full subdispersion case, i.e. $\forall s \in (0,1]$. It is also interesting to explore similar equations for the superdispersion case $s>1$.

Remark 4.2. We also remark here that it might be interesting to derive the dynamical laws for the condensate width δ_ν which is defined as

$$\delta_\nu(t) = \int_{\mathbb{R}^d} \nu^2 |\psi(\mathbf{x})|^2 d\mathbf{x}, \qquad \nu = x, y \text{ in 2D and } \nu = x, y, z \text{ in 3D}. \tag{4.13}$$

The derivation and proof are feasible but tedious. One can refer to [55] for the analogous details.

4.2. Numerical method

In this subsection, we first introduce a coordinates transformation and reformulate the rotating FGPE (1.1)–(1.2) in the new coordinates, eliminating hence the rotation term.

4.2.1. Rotating Lagrangian coordinates transformation

For any time $t \geq 0$, let $A(t)$ be the orthogonal rotational matrix defined as [14]

$$A(t) = \begin{pmatrix} \cos(\Omega t) & \sin(\Omega t) \\ -\sin(\Omega t) & \cos(\Omega t) \end{pmatrix}, \quad \text{if } d=2, \quad A(t) = \begin{pmatrix} \cos(\Omega t) & \sin(\Omega t) & 0 \\ -\sin(\Omega t) & \cos(\Omega t) & 0 \\ 0 & 0 & 1 \end{pmatrix}, \quad \text{if } d=3. \tag{4.14}$$

It is easy to check that $A^{-1}(t) = A^T(t)$ for any $t \geq 0$ and $A(0) = I$, where I is the identity matrix. For any $t \geq 0$, we introduce the *rotating Lagrangian coordinates* $\widetilde{\mathbf{x}}$ as [8,14]

$$\widetilde{\mathbf{x}} = A^{-1}(t)\mathbf{x} = A^T(t)\mathbf{x} \quad \Leftrightarrow \quad \mathbf{x} = A(t)\widetilde{\mathbf{x}}, \qquad \mathbf{x} \in \mathbb{R}^d, \tag{4.15}$$

and we denote by $\phi := \phi(\widetilde{\mathbf{x}}, t)$ the wave function in the new coordinates

$$\phi(\widetilde{\mathbf{x}}, t) := \psi(\mathbf{x}, t) = \psi\left(A(t)\widetilde{\mathbf{x}}, t\right), \qquad \mathbf{x} \in \mathbb{R}^d, \quad t \geq 0. \tag{4.16}$$

By some simple calculations, one can easily obtain

$$\partial_t \phi(\widetilde{\mathbf{x}}, t) = \partial_t \psi(\mathbf{x}, t) + \nabla\psi(\mathbf{x}, t) \cdot \left(\dot{A}(t)\widetilde{\mathbf{x}}\right) = \partial_t \psi(\mathbf{x}, t) - \Omega(x\partial_y - y\partial_x)\psi(\mathbf{x}, t), \tag{4.17}$$

$$(-\nabla^2 + m^2)^s \psi(\mathbf{x}, t) = (-\nabla^2 + m^2)^s \phi(\widetilde{\mathbf{x}}, t). \tag{4.18}$$

Plugging them back into (1.1)–(1.2) gives the following FNLSE in the rotating Lagrangian coordinates

$$i\partial_t \phi(\widetilde{\mathbf{x}}, t) = \left[\frac{1}{2}(-\nabla^2 + m^2)^s + \mathcal{W}(\widetilde{\mathbf{x}}, t) + \beta|\phi|^2 + \lambda\widetilde{\Phi}(\widetilde{\mathbf{x}}, t)\right]\phi(\widetilde{\mathbf{x}}, t), \quad \widetilde{\mathbf{x}} \in \mathbb{R}^d, \quad t > 0, \tag{4.19}$$

$$\widetilde{\Phi}(\widetilde{\mathbf{x}}, t) = \widetilde{\mathcal{U}} * |\phi|^2, \qquad \widetilde{\mathbf{x}} \in \mathbb{R}^d, \quad t \geq 0. \tag{4.20}$$

Here, $\mathcal{W}(\widetilde{\mathbf{x}}, t) = V(A(t)\widetilde{\mathbf{x}})$ and $\widetilde{\mathcal{U}}(\widetilde{\mathbf{x}}, t)$ reads as

$$\widetilde{\mathcal{U}}(\widetilde{\mathbf{x}},t)=\begin{cases}\frac{1}{2^{d-1}\pi|\widetilde{\mathbf{x}}|^{\mu}}, & 0<\mu<d-1, \quad \text{Coulomb},\\ -\delta(\widetilde{\mathbf{x}})-3\,\partial_{\mathbf{m}(t)\mathbf{m}(t)}\left(\frac{1}{4\pi|\widetilde{\mathbf{x}}|}\right), & \text{3D DDI},\\ -\frac{3}{2}\left(\partial_{\mathbf{m}_\perp(t)\mathbf{m}_\perp(t)}-m_3^2\nabla_\perp^2\right)\left(\frac{1}{2\pi|\widetilde{\mathbf{x}}|}\right), & \text{2D DDI},\end{cases} \tag{4.21}$$

with $\mathbf{m}(t)\in\mathbb{R}^3$ defined as $\mathbf{m}(t)=A^{-1}(t)\mathbf{n}=:\big((m_1(t),m_2(t),m_3(t)\big)^T$ and $\mathbf{m}_\perp(t)=\big(m_1(t),m_2(t)\big)^T$.

We can clearly see that the rotation term vanishes in the new coordinates (see (4.19)). Instead, the trapping potential and the dipole axis become time-dependent. The absence of the rotating term allows us to develop a simple and efficient time-splitting scheme.

4.2.2. A time-splitting pseudo-spectral method

Here we shall consider the new equation (4.19)–(4.20). In a practical computation, we first truncate the problem into a bounded computational domain $\mathbf{B}=[L_{\widetilde{x}},R_{\widetilde{x}}]\times[L_{\widetilde{y}},R_{\widetilde{y}}]\times[L_{\widetilde{z}},R_{\widetilde{z}}]$ if $d=3$, or $\mathbf{B}=[L_{\widetilde{x}},R_{\widetilde{x}}]\times[L_{\widetilde{y}},R_{\widetilde{y}}]$ if $d=2$. From $t=t_n$ to $t=t_{n+1}:=t_n+\Delta t$, the equation is solved in two steps. One first considers

$$i\partial_t\phi(\widetilde{\mathbf{x}},t)=\Big[\mathcal{W}(\widetilde{\mathbf{x}},t)+\beta|\phi|^2+\lambda\widetilde{\Phi}(\widetilde{\mathbf{x}},t)\Big]\phi(\widetilde{\mathbf{x}},t),\qquad \widetilde{\mathbf{x}}\in\mathbf{B},\quad t_n\le t\le t_{n+1}, \tag{4.22}$$

$$\widetilde{\Phi}(\widetilde{\mathbf{x}},t)=\big(\widetilde{\mathcal{U}}*\widetilde{\rho}\big)(\widetilde{\mathbf{x}},t),\qquad \widetilde{\mathbf{x}}\in\mathbf{B},\quad t_n\le t\le t_{n+1}, \tag{4.23}$$

for a time step Δt, then solves

$$i\partial_t\phi(\widetilde{\mathbf{x}},t)=\frac{1}{2}(-\nabla^2+m^2)^s\phi(\widetilde{\mathbf{x}},t),\qquad \widetilde{\mathbf{x}}\in\mathbf{B},\qquad t_n\le t\le t_{n+1}, \tag{4.24}$$

with periodic boundary conditions on the boundary $\partial\mathbf{B}$ for the same time step. Here, $\widetilde{\rho}(\widetilde{\mathbf{x}},t)=|\phi(\widetilde{\mathbf{x}},t)|^2$ if $\widetilde{\mathbf{x}}\in\mathbf{B}$ and $\widetilde{\rho}(\widetilde{\mathbf{x}},t)=0$ otherwise. The linear subproblem (4.24) is discretized in space by the Fourier pseudo-spectral method and integrated in time exactly in the phase space. The nonlinear subproblem (4.22)–(4.23) preserves the density pointwise, i.e. $|\phi(\widetilde{\mathbf{x}},t)|^2\equiv|\phi(\widetilde{\mathbf{x}},t=t_n)|^2=|\phi^n(\widetilde{\mathbf{x}})|^2$, and it can be integrated exactly as

$$\phi(\widetilde{\mathbf{x}},t)=\exp\left\{-i\Big[(t-t_n)\beta|\phi^n(\widetilde{\mathbf{x}})|^2+\lambda\boldsymbol{\varphi}(\widetilde{\mathbf{x}},t)+P(\widetilde{\mathbf{x}},t)\Big]\right\},\quad \widetilde{\mathbf{x}}\in\mathbf{B},\quad t_n\le t\le t_{n+1}, \tag{4.25}$$

$$\boldsymbol{\varphi}(\widetilde{\mathbf{x}},t)=\int_{\mathbb{R}^d}\widetilde{\mathcal{K}}(\widetilde{\mathbf{x}}-\widetilde{\mathbf{y}},t)\rho(\widetilde{\mathbf{y}},t_n)d\widetilde{\mathbf{y}}, \tag{4.26}$$

where the time-dependent kernel $\widetilde{\mathcal{K}}(\widetilde{\mathbf{x}},t)$ has the form

$$\widetilde{\mathcal{K}}(\widetilde{\mathbf{x}},t)=\int_{t_n}^{t}\widetilde{\mathcal{U}}(\widetilde{\mathbf{x}},\tau)d\tau=\begin{cases}(t-t_n)/(2^{d-1}\pi|\widetilde{\mathbf{x}}|^{\mu}), & \text{Coloumb},\\ -\delta(\widetilde{\mathbf{x}})(t-t_n)-3\widetilde{L}_3(t)(\frac{1}{4\pi|\widetilde{\mathbf{x}}|}), & \text{3D DDI},\\ -\frac{3}{2}\widetilde{L}_2(t)(\frac{1}{2\pi|\widetilde{\mathbf{x}}|}), & \text{2D DDI}.\end{cases} \tag{4.27}$$

Here, the differential operators $\widetilde{L}_3(t)=\int_{t_n}^{t}\partial_{\mathbf{m}(\tau)\mathbf{m}(\tau)}d\tau$ and $\widetilde{L}_2(t)=\int_{t_n}^{t}\left(\partial_{\mathbf{m}_\perp(\tau)\mathbf{m}_\perp(\tau)}-m_3^2\nabla_\perp^2\right)d\tau$ can be actually integrated analytically and have some explicit expressions. One can refer to *section 4.1* in [14] for more details. The GauSum solver is then applied to evaluate the nonlocal nonlinear interaction $\boldsymbol{\varphi}(\widetilde{\mathbf{x}},t)$ (4.26). In addition, we have

$$P(\widetilde{\mathbf{x}},t)=\int_{t_n}^{t}\mathcal{W}(\widetilde{\mathbf{x}},\tau)d\tau=\int_{t_n}^{t}V(A(\tau)\widetilde{\mathbf{x}})d\tau. \tag{4.28}$$

If $V(\mathbf{x})$ is chosen as the harmonic potential (1.4), then $P(\widetilde{\mathbf{x}},t)$ can be calculated analytically. For a general potential, a numerical quadrature can be used to approximate the integral (4.28).

To simplify the notations, we only present the scheme for the 2D case. Let L and M be two even positive integers. We choose $h_{\widetilde{x}}=\frac{R_{\widetilde{x}}-L_{\widetilde{x}}}{L}$ and $h_{\widetilde{y}}=\frac{R_{\widetilde{y}}-L_{\widetilde{y}}}{M}$ as the spatial mesh sizes in the $\widetilde{x}$- and $\widetilde{y}$-directions, respectively. We define the indices and grid points sets as

$$\mathcal{T}_{LM}=\Big\{(\ell,m)\in\mathbb{N}^2\,|\,0\le\ell\le L,\ 0\le m\le M\Big\},$$

$$\widetilde{\mathcal{T}}_{LM}=\Big\{(p,q)\in\mathbb{N}^2\,|\,-L/2\le p\le L/2-1,\ -M/2\le q\le M/2-1\Big\},$$

$$\mathcal{G}_{\widetilde{x}\widetilde{y}}=\big\{(\widetilde{x}_\ell,\widetilde{y}_m)=:(L_x+\ell\,h_x,L_y+m\,h_y),\ (\ell,m)\in\mathcal{T}_{LM}\big\}.$$

We introduce the following functions

$$W_{pq}(\widetilde{x},\widetilde{y})=e^{i\mu_p^{\widetilde{x}}(\widetilde{x}-L_{\widetilde{x}})}\,e^{i\mu_q^{\widetilde{y}}(\widetilde{y}-L_{\widetilde{y}})},\quad (p,q)\in\widetilde{\mathcal{T}}_{LM},$$

Table 1
Spatial errors (upper parts) $e_{\psi}^{h,\,\Delta t_0}(t)$ and temporal errors (lower parts) $e_{\psi}^{h_0,\,\Delta t}(t)$ at $t=0.4$ for the dynamics of the 2D FGPE with $\lambda=0$ and different fractional order s.

$e_{\psi}^{h,\,\Delta t_0}(t)$	$h=3/4$	$h/2$	$h/4$	$h/8$	$h/16$
$s=0.6$	1.46	6.93E−1	6.19E−2	4.40E−4	6.29E−8
$s=0.9$	1.36	3.05E−1	1.98E−2	7.45E−6	1.55E−11
$s=1.2$	8.33E−1	3.66E−2	1.19E−5	1.04E−7	5.61E−9
$e_{\psi}^{h_0,\,\Delta t}(t)$	$\Delta t=0.02$	$\Delta t/2$	$\Delta t/4$	$\Delta t/8$	$\Delta t/16$
$s=0.6$	6.58E−3	1.63E−3	4.08E−4	1.02E−4	2.53E−5
$s=0.9$	4.76E−3	1.18E−3	2.93E−4	7.31E−5	1.82E−5
$s=1.2$	7.85E−3	1.85E−3	4.56E−4	1.14E−4	2.83E−5

with

$$\mu_p^{\widetilde{x}}=\frac{2\pi p}{R_{\widetilde{x}}-L_{\widetilde{x}}},\quad \mu_q^{\widetilde{y}}=\frac{2\pi q}{R_{\widetilde{y}}-L_{\widetilde{y}}},\quad (p,q)\in\widetilde{\mathcal{T}}_{LM}.$$

Let $f_{\ell m}^n$ ($f=\phi$, $\boldsymbol{\varphi}$ or P) be the approximation of $f(\widetilde{x}_\ell,\widetilde{y}_m,t_n)$ for $(\ell,m)\in\mathcal{T}_{LM}$ and $n\geq 0$. We denote by $\boldsymbol{\phi}^n$ the solution at time $t=t_n$, with components $\{\phi_{\ell m}^n,(\ell,m)\in\mathcal{T}_{LM}\}$. We take the initial data as $\phi_{\ell m}^0=\phi_0(\widetilde{x}_\ell,\widetilde{y}_m)$, for $(\ell,m)\in\mathcal{T}_{LM}$. A second-order time-splitting Fourier pseudo-spectral (TSFP) method to solve (4.19)–(4.20) is given by

$$\phi_{\ell m}^{(1)}=\sum_{p=-L/2}^{L/2-1}\sum_{q=-M/2}^{M/2-1}e^{-\frac{i\Delta t}{4}\left[(\mu_p^{\widetilde{x}})^2+(\mu_q^{\widetilde{y}})^2+m^2\right]^s}\widehat{(\boldsymbol{\phi}^n)}_{pq}\,W_{pq}(\widetilde{x}_\ell,\widetilde{y}_m),\tag{4.29}$$

$$\phi_{\ell m}^{(2)}=\phi_{\ell m}^{(1)}\exp\left\{-i\left[\Delta t\beta|\phi_{\ell m}^{(1)}|^2+\lambda\boldsymbol{\varphi}_{\ell m}^{n+1}+P_{\ell m}^{n+1}\right]\right\},\tag{4.30}$$

$$\phi_{\ell m}^{n+1}=\sum_{p=-L/2}^{L/2-1}\sum_{q=-M/2}^{M/2-1}e^{-\frac{i\Delta t}{4}\left[(\mu_p^{\widetilde{x}})^2+(\mu_q^{\widetilde{y}})^2+m^2\right]^s}\widehat{(\boldsymbol{\phi}^{(2)})}_{pq}\,W_{pq}(\widetilde{x}_\ell,\widetilde{y}_m).\tag{4.31}$$

Here, $\widehat{(\boldsymbol{\phi}^n)}_{pq}$ and $\widehat{(\boldsymbol{\phi}^{(2)})}_{pq}$ are the discrete Fourier series coefficients of the vectors $\boldsymbol{\phi}^n$ and $\boldsymbol{\phi}^{(2)}$, respectively. This method is referred to as *TS2-GauSum*. The *TS2-GauSum* method (4.29)–(4.31) is explicit, efficient, simple to implement, unconditionally stable and can be easily extended to high-order time-splitting schemes.

4.3. Numerical results

4.3.1. Accuracy test

In this subsection, we test the accuracy of the method *TS2-GauSum* (4.29)–(4.31). To this end, we consider the 2D rotating FGPE with harmonic potential (1.4) and DDI. The parameters are chosen as $d=2$, $\beta=100$, $\Omega=0.5$ and $\gamma_x=\gamma_y=1$. The dipole axis is $\mathbf{n}=(1,0,0)^T$, while the initial data $\psi_0(\mathbf{x})$ and computational domain $\mathbf{B}$ are respectively given by

$$\psi_0(\mathbf{x})=\frac{2^{1/4}}{\sqrt{\pi}}e^{-\frac{2x^2+y^2}{2}},\qquad \mathbf{x}\in\mathbf{B}=[-12,12]\times[-12,12].\tag{4.32}$$

To demonstrate the results, we denote $\psi_{h,\,\Delta t}^n$ as the numerical approximation of $\psi(\mathbf{x},t=t_n)$ obtained by the *TS2-GauSum* (4.29)–(4.31) with mesh size $h_x=h_y=h$ and time step Δt. We take the reference ("exact") solution $\psi(\mathbf{x},t=t_n)$ as its numerical approximation obtained with very fine mesh sizes, i.e., $\psi_{h_0,\,\Delta t_0}^n$ with $h_0=\frac{3}{128}$ and $\Delta t=0.0001$. The error function is defined as follows

$$e_{\psi}^{h,\,\Delta t}(t_n):=\frac{\|\psi_{h_0,\,\Delta t_0}^n-\psi_{h,\,\Delta t}^n\|_{l^2}}{\|\psi_{h_0,\,\Delta t_0}^n\|_{l^2}},\qquad n\geq 0,\tag{4.33}$$

where $\|\cdot\|_{l^2}$ denotes the discrete l^2-norm. Table 1 shows the error functions for the FGPE with $\lambda=0$ and different s, while Table 2 reports those for the FGPE with $s=1.2$ and different λ at time $t=0.4$. From Tables 1–2, we can clearly see the *TS2-GauSum* method is spectral-order accurate in space and second-order accurate in time.

4.3.2. Dynamics simulation

In this subsection, we present some numerical results for the dynamics of the FNLSE/FGPE solved by *TS2-GauSum*. To this end, unless stated otherwise, we let $m=0$, $d=2$ and choose the computational domain as $\mathbf{B}=[-16,16]\times[-16,16]$. The mesh sizes in space and time are chosen as $h_x=h_y=\frac{1}{8}$ and $\Delta t=10^{-3}$, respectively. The trapping potential $V(\mathbf{x})$ is chosen

Table 2
Spatial errors (upper parts) $e_{\psi}^{h,\,\Delta t_0}(t)$ and temporal errors (lower parts) $e_{\psi}^{h_0,\,\Delta t}(t)$ at $t = 0.4$ for the dynamics of the 2D FGPE with $s = 1.2$ and different strength of DDI λ.

$e_{\psi}^{h,\,\Delta t_0}(t)$	$h = 3/4$	$h/2$	$h/4$	$h/8$	$h/16$
$\lambda = 1$	1.10	1.00E−1	2.13E−4	3.59E−9	1.65E−10
$\lambda = 5$	1.26	1.24E−1	5.49E−4	1.03E−8	4.57E−10
$\lambda = 10$	1.38	1.54E−1	1.27E−3	2.84E−8	1.17E−9
$e_{\psi}^{h_0,\,\Delta t}(t)$	$\Delta t = 0.02$	$\Delta t/2$	$\Delta t/4$	$\Delta t/8$	$\Delta t/16$
$\lambda = 1$	6.51E−3	1.56E−3	3.88E−4	9.66E−5	2.40E−5
$\lambda = 5$	8.08E−3	1.84E−3	4.55E−4	1.13E−4	2.82E−5
$\lambda = 10$	1.33E−2	2.24E−3	5.46E−4	1.36E−4	3.38E−5

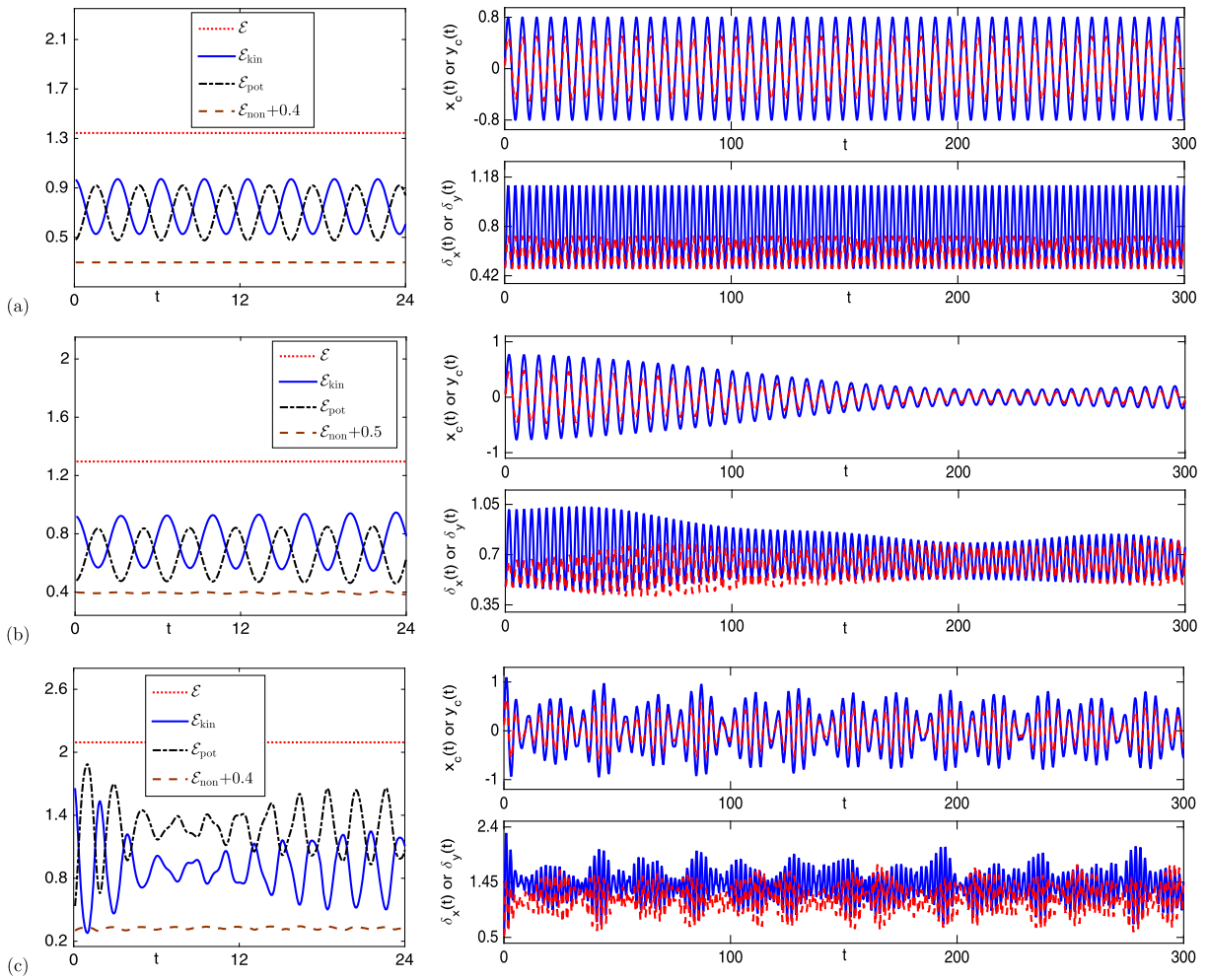

Fig. 6. Time evolution of the energies, center of mass and condensate width in Example 4.1 for case I for: (a) $s = 1$ (standard case), (b) $s = 0.95$ (subdispersion case) and (c) $s = 1.5$ (superdispersion case).

as (1.4) with $\gamma_x = \gamma_y = 1$. The nonlocal interaction is chosen as Coulomb-type with $\mu = 1$ for Examples 4.1 and 4.2, while it is taken as DDI for Example 4.3. The initial data is set to

$$\psi_0(\mathbf{x}) = \phi_g^{s_0}(\mathbf{x} - \mathbf{x}_0)\, e^{iv_0(0.8x+0.5y)}, \tag{4.34}$$

where $\phi_g^{s_0}$ is the ground state of the FNLSE with the fractional order s_0 and other parameters specified in those corresponding examples below. Starting from the ground state $\phi_g^{s_0}(\mathbf{x})$, we shift it by $\mathbf{x}_0 \in \mathbb{R}^2$ and/or imprint an initial momentum as shown above.

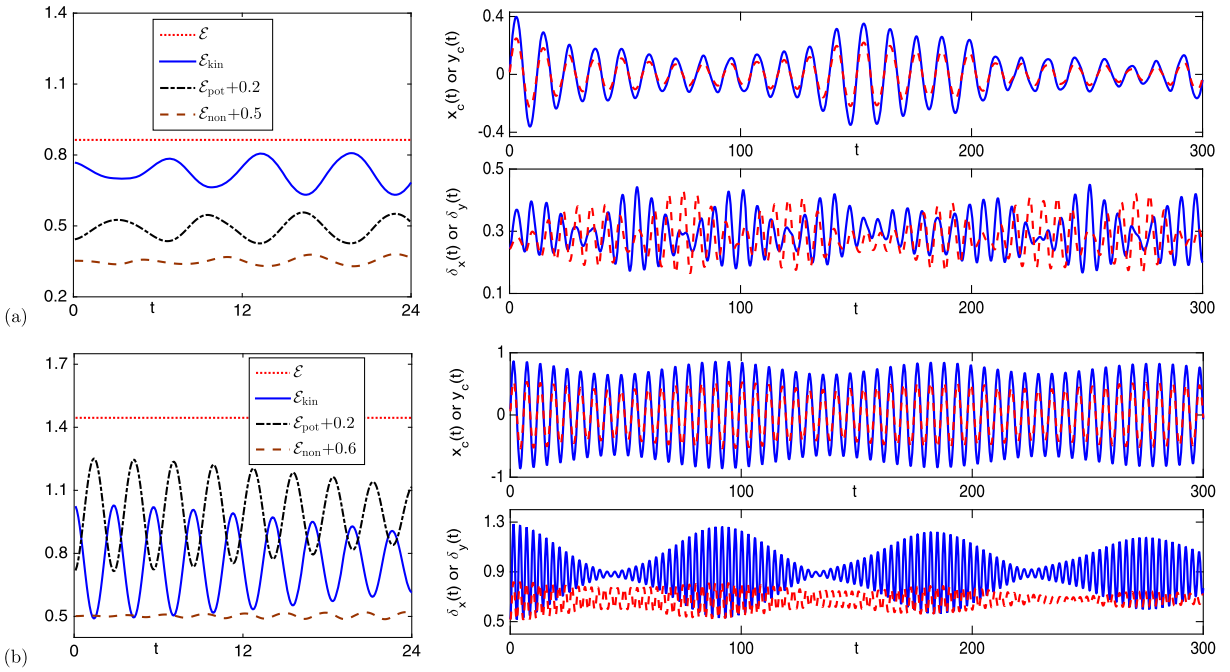

Fig. 7. Time evolution of the energies, center of mass and condensate width in Example 4.1 for case II for: (a) $s = 0.5$ (subdispersion case), (b) $s = 1.1$ (superdispersion case).

Example 4.1 *(Dynamics of the FNLSE).* ($\mathbf{x}_0 = (0, 0)^T$). In this example, let $\beta = \Omega = 0$, $\lambda = -1$, $v_0 = 1$ and $\mathbf{x}_0 = (0, 0)^T$ in (4.34). We study two cases in (4.34): **Case I:** $s_0 = 1$, **Case II:** $s_0 = s$.

Figs. 6 and 7 show the dynamics of mass, energy, center of mass, condensate widths of the FNLSE with different fractional orders s. We can observe that (i) The mass and total energy are well conserved. (ii) The fractional order significantly affects the dynamics of the FNLSE. As we know, for the classical NLSE ($s = 1$), the density profile retains its initial shape, meanwhile swings periodically in the harmonic trap (cf. Fig. 6 (a)). However, for the fractional case ($s \neq 1$), the density profile is quite different from the initial profile. For the subdispersion case, $s < 1$, the decoherence emerges, i.e. the loss of solitary profile, and it becomes stronger when $|s-1|$ is larger. For superdispersion, i.e. $s > 1$, there is much less decoherence observed. The density profile would exhibit damped oscillations around what appears to be a rescaled ground state, which behaves similarly as the breather solutions of the classical NLSE. (iii) For both cases, the decoherence is weak and turbulence (the high frequencies) does not emerge, letting alone the chaotic dynamics. The turbulence and/or chaotic dynamics might emerge if the initially imprinted momentum is large enough.

Example 4.2 *(Dynamics of the FNLSE with position shifts in initial data).* Let $\Omega = 0$. With fixed $s = s_0 = 0.75$ (subdispersion) and $v_0 = 0$ in (4.34), we study the following four cases:

- **Case I**. Linear fractional Schrödinger equation. Let $\beta = \lambda = 0$, $\mathbf{x}_0 = (1, 1)^T$.
- **Case II**. Linear fractional Schrödinger equation. Let $\beta = \lambda = 0$, $\mathbf{x}_0 = (3, 3)^T$.
- **Case III**. FNLSE with purely short-range interaction. Let $\beta = 50$, $\lambda = 0$, $\mathbf{x}_0 = (3, 3)^T$.
- **Case IV**. FNLSE with purely long-range interaction. Let $\beta = 0$, $\lambda = 10$, $\mathbf{x}_0 = (3, 3)^T$.

Fig. 8 shows the dynamics of the mass, energy, center of mass, condensate widths, while Fig. 9 shows the contour plot of the density $|\psi(\mathbf{x}, t)|^2$ at different times. Similarly to Example 4.1, we can see that (i) For the FNLSE, the density profile no longer retains its initial shape as in the classical NLSE. The density profile also oscillates around the center of the trap and decoherence emerges. (ii) The dynamics of the wave function depends crucially on the initial shift $\mathbf{x}_0$. If the initial shift is small, the initial shape is changed slightly, i.e. the decoherence is small (cf. Fig. 9 (a)), while for large shifts, the decoherence appears very quickly. Turbulence and chaotic dynamics might also occur for a large $\mathbf{x}_0$ in the linear FSE (cf. Fig. 9 (b)). (iii) Both the short- and long-range nonlinear interactions can reduce and/or delay the emergence of decoherence and suppress the wave function from chaotic dynamics. Turbulence emerges in the FNLSE with pure local nonlinearity (see Fig. 9 (c)), while the decoherence is weaker in the FNLSE with pure nonlocal nonlinearity. The density profile would actually oscillate like a breather (cf. Fig. 9 (d)). It would also be interesting to investigate the decoherence and turbulence properties in the

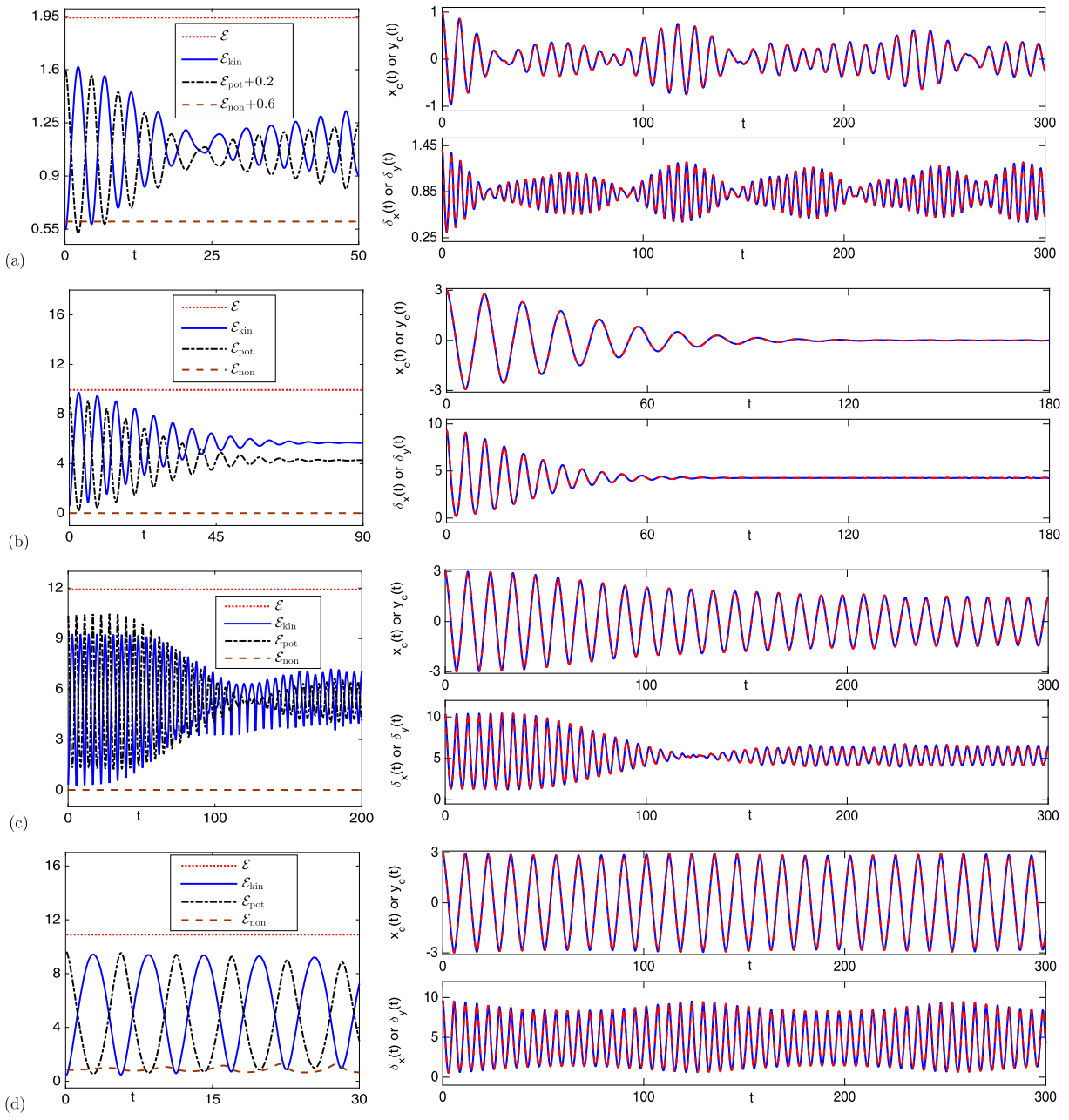

Fig. 8. Time evolution of the energies, center of mass and condensate width in Example 4.2 for cases I to IV (from top to bottom). Here, we consider a subdispersion case for $s = s_0 = 0.75$.

superdispersion case $s > 1$ and analyze how they are affected through a rotation effect. This will be considered in future research. Our results are in accordance with those reported in [44].

Example 4.3 *(Dynamics of the vortex lattice).* In (4.34), choose $v_0 = 0$ and $\phi_g^{s_0}$ as the ground state of the FNLSE with parameters $s = s_0 = 1.2$, $\Omega = 1.35$, $\beta = 100$ and $\lambda = 0$. The contour plot of $|\psi_g^{s_0}|^2$ is shown in Fig. 4 (first one in third row). With this initial data, we carry out the following five cases:

- **Case I**. Perturb the trapping frequency in both $x-$ and $y-$ directions: $\gamma_x = \gamma_y = 1.5$.
- **Case II**. Perturb the fractional order to a subdispersion one: $s = 0.7$.
- **Case III**. Perturb the fractional order to a superdispersion one: $s = 1.5$.
- **Case IV**. Turn on the dipole interaction by setting $\lambda = 80$ with dipole axis $\mathbf{n} = (1, 0, 0)$.

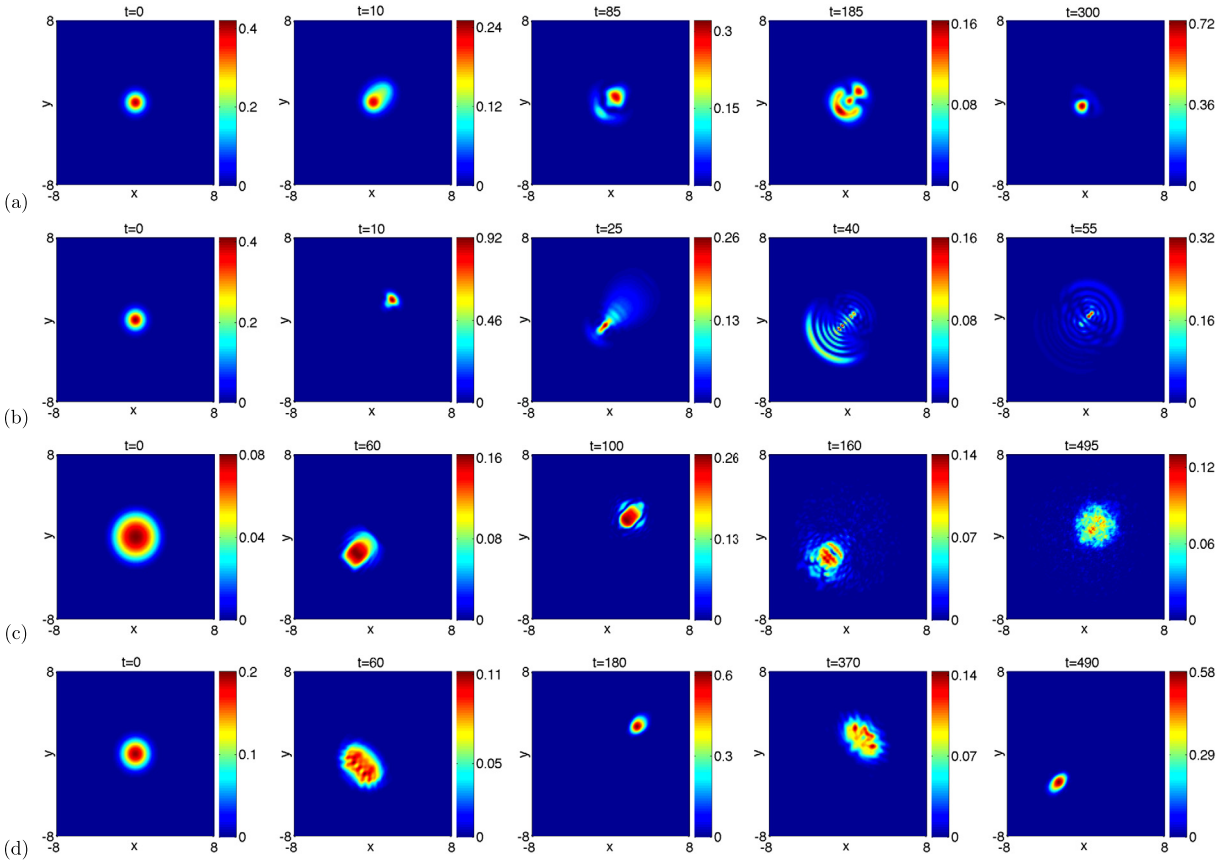

Fig. 9. Contour plots of the density $|\psi(\mathbf{x},t)|^2$ at different times in Example 4.2 for cases I to IV (from top to bottom). Here, we consider $s_0 = 0.75$ (subdispersion).

Fig. 10 depicts the contour plot of the density $|\psi(\mathbf{x},t)|^2$ at different times. Form this example and other additional numerical results, we can see that: (i) In an isotropic trapping potential, i.e. $\gamma_x = \gamma_y$, the lattices rotate around the origin and keep the similar symmetry and pattern as the initial one. In addition, the lattices also undergo a breather-like dynamics (cf. Fig. 10 (a)). While if $\gamma_x \neq \gamma_y$, symmetry breaking of the lattices would show up and the lattices rotate to form a different pattern. The number of vortices is conserved in both situation. (ii) While the fractional order is perturbed, breather-like behavior of the lattices appears. Meanwhile, decoherence/turbulence emerges if the fractional order is perturbed too much and the vortex structure is destroyed (cf. Fig. 10 (b) & (c)). (iii) While the DDI is present, the lattices pattern changes during the dynamics. The lattices rotate and redistribute according to the dipole axis.

5. Conclusion

In this paper, we proposed efficient and robust numerical methods for computing the ground states and dynamics of the FNLSE equation with an angular momentum and nonlocal interaction potentials. Existence and non-existence of the ground states were presented and dynamical laws for the mass, energy, angular momentum and center of mass were obtained.

We then studied the ground states and dynamics of the FNLSE numerically. It was found that the fractional order s affects both the ground states and dynamics in a significant way. The ground states become more peaked as $s < 1$ tends smaller, corresponding here to subdispersion. For the superdispersion case, i.e. $s > 1$, the creation of a giant vortex can be observed for a fast rotating system, which is totally different from the behavior of the classical GPE. Critical values of the rotating frequencies to create the first vortex solution are numerically found to be dependent on s. The vortex lattice pattern depends on both s and Ω. For the dynamics, decoherence as well as turbulence were observed when an initial data is prepared from a ground state with imprinted phase shift and/or position shift. It is shown that the smaller the fractional order s is, the easier the decoherence emerges. The larger the initial shift is, the easier the turbulence and chaotic dynamics arise. Furthermore, the presence of repulsive nonlinearities, both local and nonlocal, can suppress the "peaking" effects of the ground states and the decoherence/turbulence observed in the dynamics.

It is worthwhile to remark that the ground states of the FNLSE decay only algebraically as $|\mathbf{x}| \to \infty$ when the external potential $V(\mathbf{x})$ is bounded [33] and $\beta < 0$. A very large computational domain is necessary for both the ground state

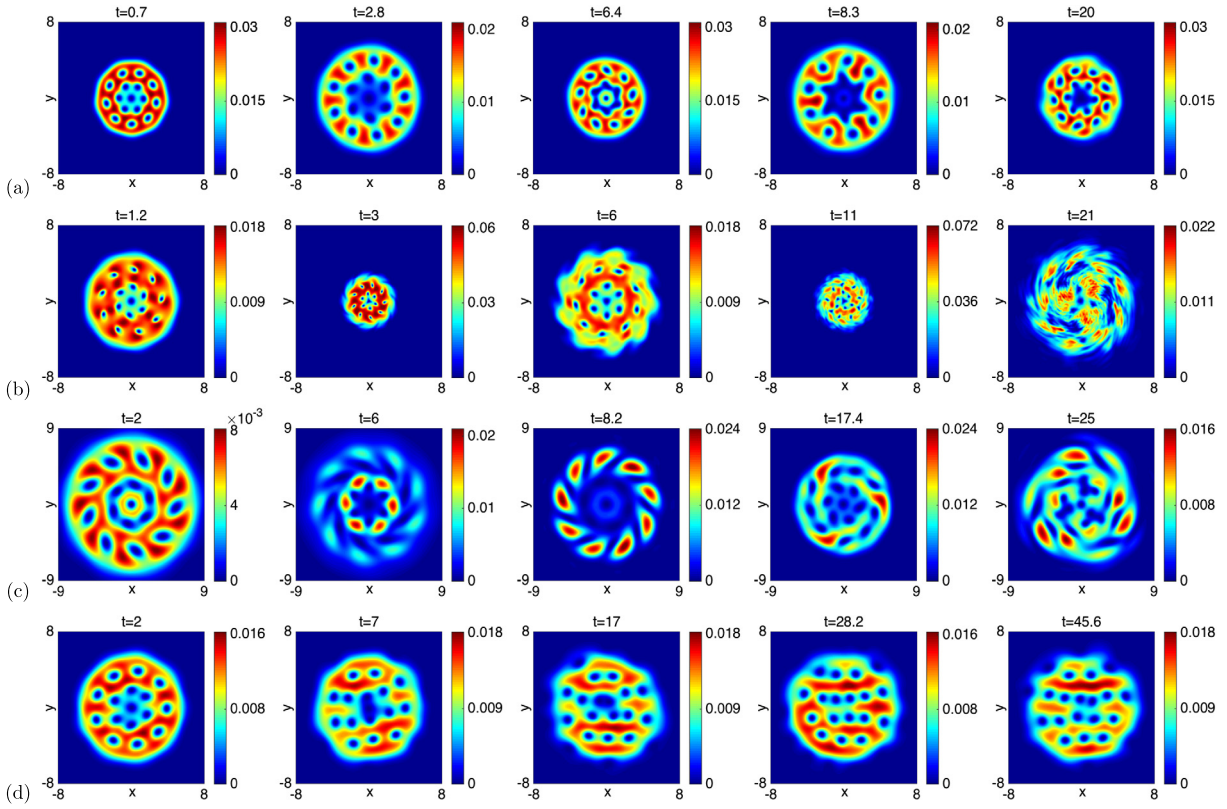

Fig. 10. Contour plots of the density $|\psi(\mathbf{x},t)|^2$ at different times in Example 4.3 for cases I to IV (from top to bottom).

computation and the dynamics [45]. It would be interesting and crucial to derive a fractional version of the free boundary conditions such as the transient BC, absorbing BC and also the PML [2] for the FNLSE.

Finally, let us emphasize that the time and space fractional NLSE, for $0 < \gamma < 1$,

$$i\partial_t^\gamma \psi(\mathbf{x},t) = \left[\frac{1}{2}\left(-\nabla^2 + m^2\right)^s + V(\mathbf{x}) + \beta|\psi(\mathbf{x},t)|^2 + \lambda\Phi(\mathbf{x},t) - \Omega L_z\right]\psi(\mathbf{x},t), \tag{5.35}$$

$$\Phi(\mathbf{x},t) = \mathcal{U} * |\psi(\mathbf{x},t)|^2, \qquad \mathbf{x}\in\mathbb{R}^d,\ t>0,\ d\geq 2 \tag{5.36}$$

is also very interesting for some applications [29,47,50,59]. The next step of our work would consist in analyzing efficient and accurate numerical methods for solving FNLSEs both in space and time and understand their behavior and properties.

Acknowledgements

We acknowledge the support from the ANR project BECASIM ANR-12-MONU-0007-02 (X. Antoine and Q. Tang), the ANR-FWF Project Lodiquas ANR-11-IS01-0003, the ANR project Moonrise ANR-14-CE23-0007-01 and the Natural Science Foundation of China grants 11261065, 91430103 and 11471050 (Y. Zhang). We are also grateful to Prof. Weizhu Bao and Dr. Yongyong Cai for valuable suggestions.

Appendix A. Proof of Lemma 4.1

Let us introduce $\mathbf{k} = (k_1,k_2,k_3)^T$ if $d=3$, and $\mathbf{k} = (k_1,k_2)^T$ if $d=2$. Let $J_z = y\partial_x - x\partial_y$ and $\widehat{J}_z = k_2\partial_{k_1} - k_1\partial_{k_2}$. Then, we have $\widehat{J_z\psi} = \widehat{J}_z\,\widehat{\psi}$. Differentiating (4.2), noticing (1.1) and using the Plancherel's formula, we have

$$\begin{aligned}\frac{d}{dt}\langle L_z\rangle(t) &= \langle L_z\psi_t,\psi\rangle + \langle L_z\psi,\psi_t\rangle = -\langle i\psi_t, J_z\psi\rangle - \langle J_z\psi, i\psi_t\rangle \\ &= \frac{1}{(2\pi)^d}\left\{-\langle\,\frac{1}{2}\left(|\mathbf{k}|^2+m^2\right)^s\widehat{\psi} + \widehat{\mathcal{V}\psi}, \widehat{J}_z\widehat{\psi}\,\rangle - \langle\,\widehat{J}_z\widehat{\psi}, \frac{1}{2}\left(|\mathbf{k}|^2+m^2\right)^s\widehat{\psi} + \widehat{\mathcal{V}\psi}\,\rangle\right\},\end{aligned} \tag{A.1}$$

with $\mathcal{V}\psi := V\psi + \lambda\Phi\,\psi$. The rotation and local nonlinear terms cancel. We omit both for brevity.

By integrating the above equation by parts, we have

$$\begin{aligned}\frac{d}{dt}\langle L_z\rangle(t) &= \frac{1}{(2\pi)^d}\left\{-\langle\frac{1}{2}\big(|\mathbf{k}|^2+m^2\big)^s\widehat{\psi}+\widehat{\mathcal{V}\psi},\widehat{J}_z\widehat{\psi}\rangle+\langle\widehat{\psi},\widehat{J}_z\left(\frac{1}{2}\big(|\mathbf{k}|^2+m^2\big)^s\widehat{\psi}+\widehat{\mathcal{V}\psi}\right)\rangle\right\}\\ &= \frac{1}{(2\pi)^d}\left\{\langle\widehat{\psi},\widehat{J}_z(\widehat{\mathcal{V}\psi})\rangle-\langle\widehat{\mathcal{V}\psi},\widehat{J}_z\widehat{\psi}\rangle\right\}=\frac{1}{(2\pi)^d}\left\{-\langle\widehat{J}_z\widehat{\psi},\widehat{\mathcal{V}\psi}\rangle-\langle\widehat{\mathcal{V}\psi},\widehat{J}_z\widehat{\psi}\rangle\right\}\\ &= -\langle J_z\psi,\mathcal{V}\psi\rangle-\langle\mathcal{V}\psi,J_z\psi\rangle=\langle|\psi|^2,\ J_z\mathcal{V}\rangle=\int_{\mathbb{R}^d}|\psi|^2(y\partial_x-x\partial_y)\Big(V(\mathbf{x})+\lambda\Phi(\mathbf{x},t)\Big)d\mathbf{x}.\end{aligned}\tag{A.2}$$

Therefore, by adapting the polar/cylindrical coordinates transformation in 2D/3D and noticing $y\partial_x-x\partial_y=-\partial_\theta$, one can obtain

$$I_1=:\int_{\mathbb{R}^d}|\psi|^2(y\partial_x-x\partial_y)V(\mathbf{x})d\mathbf{x}=0,\tag{A.3}$$

provide that $V(\mathbf{x})$ is radially/cylindrically symmetric in 2D/3D. Now that

$$I_2=:\int_{\mathbb{R}^d}|\psi|^2(y\partial_x-x\partial_y)\Phi(\mathbf{x},t)d\mathbf{x}=\frac{1}{(2\pi)^d}\widehat{\langle|\psi|^2,\ \widehat{J}_z\widehat{\Phi}\rangle}=\int_{\mathbb{R}^d}\widehat{\mathcal{U}}(\mathbf{k})\widehat{|\psi|^2}(k_2\partial_{k_1}-k_1\partial_{k_2})\widehat{|\psi|^2}d\mathbf{k},\tag{A.4}$$

applying the polar/cylindrical coordinates transformation in 2D/3D in the Fourier space, it is easily to get $I_2=0$ if $\widehat{\mathcal{U}}(\mathbf{k})$ in (1.5) is chosen as the Coulomb-type interaction or DDI with $\mathbf{n}=(0,0,1)^T$. □

Appendix B. Proof of Lemma 4.2

Step 1: By differentiating (4.5) and noticing (1.1), we have

$$\begin{aligned}\dot{\mathbf{x}}_c(t) &= \frac{d}{dt}\langle\mathbf{x}\psi,\psi\rangle=\frac{1}{i}\langle\mathbf{x}\,i\psi_t,\psi\rangle+i\langle\mathbf{x}\psi,i\psi_t\rangle=i\left[\langle\mathbf{x}\psi,i\psi_t\rangle-\langle\mathbf{x}\,i\psi_t,\psi\rangle\right]\\ &= \frac{i}{2}\Big[\langle\mathbf{x}\psi,(-\Delta+m^2)^s\psi\rangle-\langle\mathbf{x}(-\Delta+m^2)^s\psi,\psi\rangle\Big]-\Omega\left[\langle\mathbf{x}J_z\psi,\psi\rangle+\langle\psi,\mathbf{x}J_z\psi\rangle\right].\end{aligned}\tag{B.1}$$

An integration by parts and an application of Plancherel's formula lead to

$$\begin{aligned}\dot{\mathbf{x}}_c(t) &= \frac{i}{2}\frac{1}{(2\pi)^d}\left\{\langle i\nabla_{\mathbf{k}}\widehat{\psi},(|\mathbf{k}|^2+m^2)^s\widehat{\psi}\rangle-\langle i\nabla_{\mathbf{k}}[(|\mathbf{k}|^2+m^2)^s\widehat{\psi}(\mathbf{k})],\widehat{\psi}\rangle\right\}+\Omega\langle\psi J_z\mathbf{x},\psi\rangle\\ &= \frac{s}{(2\pi)^d}\langle(|\mathbf{k}|^2+m^2)^{s-1}\mathbf{k}\widehat{\psi},\widehat{\psi}\rangle+\Omega J\mathbf{x}_c.\end{aligned}\tag{B.2}$$

Note that (B.2) is well-defined for $\forall s>0$. If $s=1$, (B.2) yields

$$\dot{\mathbf{x}}_c(t)-\Omega J\mathbf{x}_c=\frac{1}{(2\pi)^d}\langle\mathbf{k}\widehat{\psi},\widehat{\psi}\rangle=i\langle\psi,\nabla\psi\rangle=i\langle G*\psi,\nabla\psi\rangle,\tag{B.3}$$

with $G(\mathbf{x})=\delta(\mathbf{x})$. If $0<s<1$, we have

$$\Big(|\mathbf{k}|^2+m^2\Big)^{s-1}=\frac{1}{c_s}\int_0^\infty\lambda^{-s}e^{-\pi(|\mathbf{k}|^2+m^2)\lambda}d\lambda,\qquad\text{with}\qquad c_s=\Gamma\big(1-s\big)/\pi^{1-s}.\tag{B.4}$$

Hence, one gets

$$\begin{aligned}&s\,\mathcal{F}^{-1}\Big(\big(|\mathbf{k}|^2+m^2\big)^{s-1}\widehat{\psi}\Big)=s\frac{1}{(2\pi)^d}\int_{\mathbb{R}^d}\Big(|\mathbf{k}|^2+m^2\Big)^{s-1}\widehat{\psi}\,e^{i\mathbf{k}\cdot\mathbf{x}}d\mathbf{k}\\ &=\frac{s}{c_s}\int_0^\infty\lambda^{-s}e^{-\pi\lambda m^2}\left[\frac{1}{(2\pi)^d}\int_{\mathbb{R}^d}\widehat{\psi}\,e^{-\pi\lambda|\mathbf{k}|^2}e^{i\mathbf{k}\cdot\mathbf{x}}d\mathbf{k}\right]d\lambda=\frac{s}{c_s}\int_0^\infty\lambda^{-s}e^{-\pi\lambda m^2}\left[\psi*\mathcal{F}^{-1}\left(e^{-\pi\lambda|\mathbf{k}|^2}\right)\right]d\lambda\\ &=\frac{s}{c_s(2\pi)^d}\int_0^\infty\lambda^{-s}e^{-\pi\lambda m^2}\int_{\mathbb{R}^d}\lambda^{-\frac{d}{2}}e^{-\frac{|\mathbf{x}-\mathbf{y}|^2}{4\pi\lambda}}\psi(\mathbf{y})d\mathbf{y}d\lambda\\ &=\frac{s}{c_s(2\pi)^d}\int_{\mathbb{R}^d}\psi(\mathbf{y})\left[\int_0^\infty\lambda^{-\frac{2s+d}{2}}e^{-\pi\lambda m^2}e^{-\frac{|\mathbf{x}-\mathbf{y}|^2}{4\pi\lambda}}d\lambda\right]d\mathbf{y}=:\Big(G*\psi\Big)(\mathbf{x}),\end{aligned}\tag{B.5}$$

with

$$G(\mathbf{x}) = \frac{s}{c_s(2\pi)^d}\int_0^\infty \lambda^{-\frac{2s+d}{2}} e^{-\pi\lambda m^2} e^{-\frac{|\mathbf{x}|^2}{4\pi\lambda}} d\lambda = \frac{2^{s-d/2}s}{\Gamma(1-s)\pi^{d/2}}\left(\frac{m}{|\mathbf{x}|}\right)^{\frac{d}{2}+s-1} K_{\frac{d}{2}+s-1}\Big(m|\mathbf{x}|\Big), \tag{B.6}$$

where $K_\nu(z)$ is the modified Bessel function of the second-kind and order ν defined by (4.10). Finally, we obtain

$$\dot{\mathbf{x}}_c(t) - \Omega J\mathbf{x}_c = \frac{s}{(2\pi)^d}\langle(|\mathbf{k}|^2+m^2)^{s-1}\mathbf{k}\widehat{\psi},\widehat{\psi}\,\rangle = \Big\langle s\mathcal{F}^{-1}\big((|\mathbf{k}|^2+m^2)^{s-1}\widehat{\psi}\big), \mathcal{F}^{-1}\big(\mathbf{k}\widehat{\psi}\big)\Big\rangle = i\big\langle(G*\psi),\nabla\psi\big\rangle. \tag{B.7}$$

Step 2: Let us consider the second-order derivative of (B.2). By (B.5), we have

$$\begin{aligned}
\ddot{\mathbf{x}}_c(t) - \Omega J\dot{\mathbf{x}}_c &= 2s\,\mathrm{Re}\Big(C_d\langle\mathbf{k}(|\mathbf{k}|^2+m^2)^{s-1}\widehat{\psi}_t,\widehat{\psi}\,\rangle\Big) = 2s\,\mathrm{Im}\Big(C_d\langle i\widehat{\psi}_t,\mathbf{k}(|\mathbf{k}|^2+m^2)^{s-1}\widehat{\psi}\,\rangle\Big)\\
&= 2\,\mathrm{Im}\Big(C_d\langle s\mathcal{F}^{-1}\Big((|\mathbf{k}|^2+m^2)^{s-1}\widehat{\mathcal{V}\psi}\Big),\,\mathcal{F}^{-1}\big(\mathbf{k}\widehat{\psi}\big)\rangle\Big) + s\,\Omega\Big[C_d\langle\widehat{\psi},\mathbf{k}(|\mathbf{k}|^2+m^2)^{s-1}\widehat{J_z\psi}\,\rangle\\
&\quad + C_d\langle\widehat{\psi},\widehat{\psi}\,\widehat{J_z}\big(\mathbf{k}(|\mathbf{k}|^2+m^2)^{s-1}\big)\rangle - C_d\langle\mathbf{k}(|\mathbf{k}|^2+m^2)^{s-1}\widehat{\psi},\widehat{J_z\psi}\,\rangle\Big]\\
&= 2\,\mathrm{Re}\Big(\big\langle G*(\mathcal{V}\psi),\nabla\psi\big\rangle\Big) + s\,\Omega\,C_d\langle(|\mathbf{k}|^2+m^2)^{s-1}\widehat{\psi},\widehat{\psi}\,\widehat{J_z}\mathbf{k}\rangle\\
&= 2\,\mathrm{Re}\Big(\big\langle G*(\mathcal{V}\psi),\nabla\psi\big\rangle\Big) + \Omega J\big(\dot{\mathbf{x}}_c - \Omega J\mathbf{x}_c\big).
\end{aligned}$$

Hence, we obtain

$$\ddot{\mathbf{x}}_c(t) - 2\Omega J\dot{\mathbf{x}}_c + \Omega^2 J^2\mathbf{x}_c = 2\,\mathrm{Re}\Big(\big\langle G*(\mathcal{V}\psi),\nabla\psi\big\rangle\Big), \tag{B.8}$$

ending hence the proof. □

References

[1] G.L. Aki, P.A. Markowich, C. Sparber, Classical limit for semi-relativistic Hartree system, J. Math. Phys. 49 (2008) 102–110.
[2] X. Antoine, A. Arnold, C. Besse, M. Ehrhardt, A. Schädle, A review of transparent and artificial boundary conditions techniques for linear and nonlinear Schrödinger equations, Commun. Comput. Phys. 4 (2008) 729–796.
[3] X. Antoine, W. Bao, C. Besse, Computational methods for the dynamics of the nonlinear Schrödinger/Gross–Pitaevskii equations, Comput. Phys. Commun. 184 (2013) 2621–2633.
[4] X. Antoine, R. Duboscq, Robust and efficient preconditioned Krylov spectral solvers for computing the ground states of fast rotating and strongly interacting Bose–Einstein condensates, J. Comput. Phys. 258 (2014) 509–523.
[5] X. Antoine, R. Duboscq, GPELab, a Matlab toolbox to solve Gross–Pitaevskii equations I: computation of stationary solutions, Comput. Phys. Commun. 185 (2014) 2969–2991.
[6] X. Antoine, R. Duboscq, GPELab, a Matlab toolbox to solve Gross–Pitaevskii equations II: dynamics and stochastic simulations, Comput. Phys. Commun. 193 (2015) 95–117.
[7] X. Antoine, R. Duboscq, Modeling and computation of Bose–Einstein condensates: stationary states, nucleation, dynamics, stochasticity, in: Nonlinear Optical and Atomic Systems: at the Interface of Mathematics and Physics, in: Lecture Notes in Mathematics, vol. 2146, Springer, 2015, pp. 49–145.
[8] P. Antonelli, D. Marahrens, C. Sparber, On the Cauchy problem for nonlinear Schrödinger equations with rotation, Discrete Contin. Dyn. Syst., Ser. A 32 (2012) 703–715.
[9] W. Bao, Y. Cai, Mathematical theory and numerical methods for Bose–Einstein condensation, Kinet. Relat. Models 6 (2013) 1–135.
[10] W. Bao, Y. Cai, H. Wang, Efficient numerical methods for computing ground states and dynamics of dipolar Bose–Einstein condensates, J. Comput. Phys. 229 (2010) 7874–7892.
[11] W. Bao, X. Dong, Numerical methods for computing ground state and dynamics of nonlinear relativistic Hartree equation for boson stars, J. Comput. Phys. 230 (2011) 5449–5469.
[12] W. Bao, H. Jian, N.J. Mauser, Y. Zhang, Dimension reduction of the Schrödinger equation with Coulomb and anisotropic confining potentials, SIAM J. Appl. Math. 73 (2013) 2100–2123.
[13] W. Bao, S. Jiang, Q. Tang, Y. Zhang, Computing the ground state and dynamics of the nonlinear Schrödinger equation with nonlocal interactions via the nonuniform FFT, J. Comput. Phys. 296 (2015) 72–89.
[14] W. Bao, D. Marahrens, Q. Tang, Y. Zhang, A simple and efficient numerical method for computing the dynamics of rotating Bose–Einstein condensates via rotating Lagrangian coordinates, SIAM J. Sci. Comput. 35 (2013) A2671–A2695.
[15] W. Bao, Q. Tang, Z. Xu, Numerical methods and comparison for computing dark and bright solitons in the nonlinear Schrödinger equation, J. Comput. Phys. 235 (2013) 423–445.
[16] W. Bao, Q. Tang, Y. Zhang, Accurate and efficient numerical methods for computing ground states and dynamics of dipolar Bose–Einstein condensates via the nonuniform FFT, arXiv:1504.02897.
[17] S.S. Bayin, On the consistency of solutions of the space fractional Schrödinger equation, J. Math. Phys. 53 (2012) 042105.
[18] S.S. Bayin, Comment on "On the consistency of solutions of the space fractional Schrödinger equation", J. Math. Phys. 54 (2013) 074101.
[19] C. Besse, G. Dujardin, I. Lacroix-Violet, High-order exponential integrators for nonlinear Schrödinger equations with application to rotating Bose–Einstein condensates, 2015, ⟨hal-01170888⟩.
[20] R. Carles, P.A. Markowich, C. Sparber, On the Gross–Pitaevskii equation for trapped dipolar quantum gases, Nonlinearity 21 (2008) 2569–2590.
[21] Y. Cho, H. Hajaiej, G. Hwang, T. Ozawa, On the Cauchy problem of fractional Schrödinger equation with Hartree type nonlinearity, Funkc. Ekvacioj 56 (2013) 193–224.
[22] Y. Cho, H. Hajaiej, G. Hwang, T. Ozawa, On the orbital stability of fractional Schrödinger equations, Commun. Pure Appl. Anal. 13 (2014) 1267–1282.
[23] Y. Cho, T. Ozawa, On the semi-relativistic Hartree-type equation, SIAM J. Math. Anal. 38 (2006) 1060–1074.

[24] V. Coti Zelati, M. Nolasco, Existence of ground states for nonlinear, pseudo-relativistic Schrödinger equations, Rend. Lincei, Mat. Appl. 22 (2011) 51–72.
[25] I. Danaila, P. Kazemi, A new Sobolev gradient method for direct minimization of the Gross–Pitaevskii energy with rotation, SIAM J. Sci. Comput. 32 (2010) 2447–2467.
[26] Q. Du, M. Gunzburger, R.B. Lehoucq, K. Zhou, Analysis and approximation of nonlocal diffusion problems with volume constraints, SIAM Rev. 54 (2012) 667–696.
[27] S. Duo, Y. Zhang, Mass-conservative Fourier spectral methods for solving the fractional nonlinear Schrödinger equation, Comput. Math. Appl. 71 (11) (2016) 2257–2271.
[28] A. Elgart, B. Schlein, Mean field dynamics of boson stars, Commun. Pure Appl. Math. 60 (2007) 500–545.
[29] H. Ertik, D. Demirhan, H. Sirin, F. Buyukkilic, Time fractional development of quantum systems, J. Math. Phys. 51 (2010) 082102.
[30] H. Ertik, H. Sirin, D. Demirhan, F. Buyukkilic, Fractional mathematical investigation of Bose–Einstein condensation in dilute ^{87}Rb, ^{23}Na and ^{7}Li atomic gases, Int. J. Mod. Phys. B 26 (2012) 1250096.
[31] L. Exl, N.J. Mauser, Y. Zhang, Accurate and efficient computation of nonlocal potentials based on Gaussian-sum approximation, arXiv:1501.04438.
[32] R.P. Feynman, A.R. Hibbs, Quantum Mechanics and Path Integrals, McGraw-Hill, New York, 1965.
[33] R.L. Frank, E. Lenzmann, Uniqueness of nonlinear ground states for fractional Laplacians in $\mathbb{R}$, Acta Math. 210 (2013) 261–318.
[34] J. Fröhlich, E. Lenzmann, Blowup for nonlinear wave equations describing boson stars, Commun. Pure Appl. Math. 60 (2007) 1691–1705.
[35] B. Guo, X. Pu, F. Huang, Fractional Partial Differential Equations and Their Numerical Solutions, World Scientific, Singapore, 2015.
[36] E. Hawkins, J.M. Schwarz, Comment on "On the consistency of solutions of the space fractional Schrödinger equation", J. Math. Phys. 54 (2013) 014101.
[37] B.I. Henry, T.A.M. Langlands, P. Straka, An introduction to fractional diffusion, in: R.L. Dewar, F. Detering (Eds.), Complex Physical, Biophysical and Econophysical Systems, in: World Scientific Lecture Notes in Complex Systems, vol. 9, World Scientific, Hackensack, NJ, 2010.
[38] Y. Hong, Y. Sire, On fractional Schrödinger equation in Sobolev spaces, Commun. Pure Appl. Anal. 14 (2015) 2265–2282.
[39] A.D. Ionescu, F. Pusateri, Nonlinear fractional Schrödinger equations in one dimension, J. Funct. Anal. 266 (2014) 139–176.
[40] M. Jeng, S.-L.-Y. Xu, E. Hawkins, J.M. Schwarz, On the nonlocality of the fractional Schrödinger equation, J. Math. Phys. 51 (2010) 062102.
[41] S. Jiang, L. Greengard, W. Bao, Fast and accurate evaluation of dipolar interaction in Bose–Einstein condensates, SIAM J. Sci. Comput. 36 (2014) B777–B794.
[42] G.E. Karniadakis, J.S. Hesthaven, I. Podlubny, Fractional PDEs theory, numerics and applications, J. Comput. Phys. 293 (2015) 1–462.
[43] K. Kirkpatrick, E. Lenzmann, G. Staffilan, On the continuum limit for discrete NLS with long-range lattice interactions, Commun. Math. Phys. 317 (2012) 563–591.
[44] K. Kirkpatrick, Y. Zhang, Fractional Schrödinger dynamics and decoherence, 2014, preprint.
[45] C. Klein, C. Sparber, P. Markowich, Numerical study of fractional nonlinear Schrödinger equations, Proc. R. Soc. A 470 (2014) 20140364.
[46] N. Laskin, Fractional quantum mechanics and Lévy path integrals, Phys. Lett. A 268 (2000) 298–304.
[47] N. Laskin, Fractional Schrödinger equation, Phys. Rev. E 66 (2002) 056108.
[48] N. Laskin, Principles of fractional quantum mechanics, arXiv:1009.5533.
[49] E.H. Lieb, M. Loss, Analysis, American Mathematical Society, 2001.
[50] M. Naber, Time fractional Schrödinger equation, J. Math. Phys. 45 (2004) 3339.
[51] I. Podlubny, Fractional Differential Equations, Mathematics in Science and Engineering, vol. 198, Academic Press, 1999.
[52] S. Secchi, Ground state solutions for nonlinear fractional Schrödinger equation in $\mathbb{R}^N$, J. Math. Phys. 54 (2013) 031501.
[53] S. Secchi, M. Squassina, Soliton dynamics for fractional Schrödinger equation, Appl. Anal. 93 (2014) 1702–1729.
[54] X. Shang, J. Zhang, Ground state for fractional Schrödinger equation with critical growth, Nonlinearity 27 (2014) 187–207.
[55] Q. Tang, Numerical studies on quantized vortex dynamics in superfluidity and superconductivity, Ph. D thesis, National University of Singapore, 2013.
[56] N. Uzar, S. Ballikaya, Investigation of classical and fractional Bose–Einstein condensation for harmonic potential, Physica A 392 (2013) 1733–1741.
[57] N. Uzar, S.D. Han, T. Tufekci, E. Aydiner, Solutions of the Gross–Pitaevskii and time fractional Gross–Pitaevskii equations for different potentials with homotopy perturbation method, arXiv:1203.3352.
[58] P. Wang, C. Huang, An energy conservative difference scheme for the nonlinear fractional Schrödinger equations, J. Comput. Phys. 293 (2015) 238–251.
[59] S. Wang, M. Xu, Generalized fractional Schrödinger equation with space-time fractional derivatives, J. Math. Phys. 48 (2007) 043502.
[60] Y. Zhang, X. Dong, On the computation of ground state and dynamics of Schrödinger–Poisson–Slater system, J. Comput. Phys. 230 (2011) 2660–2676.